UPPSALA
UNIVERSITET

Comparison of intensified turbulence events in the Baltic Sea

Linnéa Hallgren

Author:
Linnéa Hallgren

Comparison of intensified turbulence events in the Baltic Sea

Master's Programme in Environmental and Water Engineering 30hp,
VT-2021

Supervisor: Leonie Esters
Subject reader: Erik Sahlée

Datum: June 1, 2021

Abstract

Comparison of intensified turbulence events in the Baltic Sea.
Linnéa Hallgren

Turbulence is important since it affects the exchange of momentum, heat, and trace gases between the atmosphere and ocean. However, measuring oceanic turbulence is not straightforward and that is why parameterizations that describe turbulence events are important. In this thesis turbulence data from the Baltic Sea is investigated and compared to already existing parameterizations.

The thesis considers turbulence in the ocean surface boundary layer (OSBL) and how atmospheric parameters act as driving mechanisms. Turbulence creates mixing that enables the dispersion of various particles and a more efficient gas transfer at the air-sea interface. This thesis aimed to investigate the connection between the drivers of oceanic turbulence, wind, waves, and buoyancy fluxes and how they contribute to the formation of enhanced turbulence events. To investigate this, turbulence data from the Baltic Sea from June to August 2020, collected by an ADCP (Acoustic Doppler Current Profiler), was used to find connections to meteorological data during the same time period. Since turbulence is difficult to measure, three already existing parameterizations were compared to the observed turbulence to investigate their performance. The results showed that conditions with higher wind speeds with corresponding waves gave a better correlation between surface turbulence and wind and waves. The parameterization that included wind and waves gave results closest to the observed turbulence at the surfaces, compared to when only wind shear was included. It was also detected that the parameterized turbulence was in almost all cases under-predicted in comparison to the observed turbulence. To clarify why this is the case, a more detailed analysis would be needed to find what parameters are missing for better predictions of the surface turbulence.

Keywords: Turbulence, Upper ocean, Ocean mixing, Parameterization.

Department of Earth Sciences, Program for Air, Water and Landscape Science, Uppsala University, Villavägen 16, SE-75236 Uppsala, Sweden.

Referat

Jämförelse av förhöjda turbulensevent i Östersjön
Linnéa Hallgren

Turbulens är viktigt eftersom det påverkar utbytet av energi, värme och gaser mellan havet och atmosfären. Däremot är det svårt att mäta turbulens och därför är det viktigt med parametriseringar som kan beskriva turbulensevent. I denna studie analyserades turbulensdata från Östersjön som sedan jämfördes med uträknad turbulens med befintliga parametriseringar.

Det som avhandlas i denna studie är turbulens i havets gränsskikt och hur atmosfäriska parametrar fungerar som drivmekanismer för att skapa turbulens. Turbulens skapar omblandning i havet som möjliggör dispersion för partiklar samt att gasutbytet blir mer effektivt vid gränsskiktet mellan havet och atmosfären. Detta gör i sin tur att mer koldioxid kan tas upp av haven än om det inte hade funnits någon turbulens. Syftet med studien var att undersöka drivmekanismerna för oceanisk turbulens för att se hur de bidrar till skapandet av turbulens. För att undersöka detta analyserades turbulensdata från Östersjön från juni till augusti 2020, uppmätt av en ADCP (Acoustic Doppler Current Profiler). Denna data användes sedan för att hitta kopplingar till meteorologisk data under samma tidsperiod. Eftersom turbulens är svårt att mäta, undersöktes även tre parametriseringar för att se hur väl de kunde beskriva den uppmätta turbulensen. Resultaten visade att vid förhållanden med hög vindhastighet där det samtidigt fanns vågor som påvisade samma beteende visade på bättre korrelation mellan yt-turbulensen och vind och vågor. Parametriseringen som inkluderade vind och vågor, som i denna rapport kallas *Terray*, i sin uträkning gav resultat mest lik den uppmätta turbulensen. Analysen visade även att den parametriserade turbulensen för *Terray* var underskattad i alla fall förutom i ett fall. För att utreda varför detta var fallet, behövs en mer detaljerad analys utföras.

Nyckelord: Turbulens, Havets gränsskikt, Havsomblandning , Parametrisering.

Preface

This thesis was written as the conclusive part of my studies within the Master's Programme in Environmental and Water Engineering at Uppsala University and the Swedish University of Agricultural Science (SLU). Data for this research project was provided from the ICOS Ocean station at Östergarnsholm, making this thesis possible to conduct. Supervisor was Leonie Esters, Researcher at Department of Earth Sciences, Program for Air, Water and Landscape Sciences; Meteorology. Erik Sahlée, Senior lecturer/Associate Professor, at the same department, has served as subject reader.

First and foremost, I would like to thank my supervisor Leonie for her ongoing engagement throughout the whole project, even though she became a mom at the beginning of the project. She has provided guidance, interesting discussions, and answers to all my questions, no matter how big or small. I would also like to thank Erik for his insight and contribution with ideas to this project.

Lastly, I would like to thank my friends and family for their encouragement and support throughout this project and the five years of studying.

Linnéa Hallgren
Uppsala, 2021.

Acknowledgement

Populärvetenskaplig sammanfattning

De flesta är medvetna om att halten koldioxid ökar i atmosfären vilket bidrar till en global temperaturökning. Haven, som täcker över 70 % av jordens yta hjälper däremot till att motverka denna process genom att de har möjlighet att ta upp koldioxid och sedan blanda det och transportera det djupare neråt. Detta sker som en följd av den turbulens som finns i haven.

Turbulens är ett tillstånd hos vattnet som innebär att vattnet rör sig i virvlar, där virvlarna går från stora till små tills de upplöses och istället övergår till att bli värme. Anledningen till att det skapas turbulens är för att energi tillförs till vattnet som en följd av kopplingen som finns mellan atmosfären och havet. Energiöverföringen kan ske genom att vind blåser över havet och skapar vågor som därefter kan brytas och på så vis överföra energin till vattnet. Turbulens gör att ytan mellan havet och atmosfären ökar och en effekt från detta är att mer koldioxid kan tas upp av havet som på hjälper till att balansera koldioxidhalten i atmosfären. Den största anledningen till varför det är viktigt med mer forskning inom turbulens är havets förmåga att ta upp koldioxid som därmed hjälper till att motverka den globala temperaturökningen. Detta gör att klimatmodeller som förutspår framtida klimatscenarion även kan förbättras med hjälp av kunskap om turbulens och hur den kan beräknas.

I denna studie har kopplingen mellan turbulens vid ytan och atmosfäriska faktorer, så som vind och vågor, undersökts för att se hur de förhåller sig till varandra. Syftet med studien har varit att försöka hitta de mekanismer som driver turbulensen vid ytan. Utöver detta har det undersökts om redan befintliga metoder för att beräkna turbulens stämmer överens med den uppmätta turbulensen. Till sist undersöktes det även om riktningen på vågorna stämde överens med riktningen på vinden, eftersom det är vinden som skapar vågorna.

Resultatet visade att det är förhållanden med höga vindhastigheter med brytande vågor som är bäst kopplade till förstärkta turbulenshändelser vid ytan. Detta kunde även visas genom att den beräknade turbulensen som inkluderade vind och vågor i sin uträkning gav ett resultat som var närmst den uppmätta turbulensen. Det visade sig även att den beräknade turbulensen i nästan alla fall var underskattad vilket visar på att något mer bidrar till ökad turbulens. Det kan annars bero på att beräkningen för turbulens som inkluderar vind och vågor enbart fungerar i förhållanden med starka vindar med vågor som följer samma mönster. Metoder för att beräkna turbulens vid lägre vind-hastigheter behöver alltså utvecklas vidare för att få mer korrekta resultat som speglar verkligheten. Utöver detta resultat kunde det även ses att det fanns en skillnad i vind- och vågriktningen. Detta tros vara en följd av att positionen där mätningarna utfördes ligger bredvid Gotland och Östergarnsholm, vilket påverkar hur vågorna skapas och trans-porteras i området.

Genom denna studien har därmed mer kunskap om hur turbulensen ser ut i Östersjön tagits fram och även vilka driv-mekanismer det är som mest påverkar yt-turbulensen. I ett större sammanhang kan detta användas för att förstå samspelet mellan atmosfären och havet bättre.

Contents

1   Introduction

Earth's surface consists of around 71 % oceans. These oceans are closely linked to the atmosphere through the transfer of momentum, heat, mass and energy on various scales at the interface (Thorpe, 2004). Because of this, the air-sea interactions have a great impact on the weather and the global climate (National Geographic, 2019). The near-surface turbulence in the ocean is created as a consequence of the air-sea interaction through three main drivers, wind, waves and buoyancy (Belcher et al., 2012). The momentum transfer occurs through wind stress that creates surface waves. These waves, and especially breaking waves, creates a further source of turbulent kinetic energy (Gargett & Grosch, 2014). Cooling of the surface leads to convection that increases turbulence, while heating of the surface oppresses it (Brainerd & Gregg, 1993).

Turbulence creates mixing and dispersion of various particles in the ocean on different scales. It increases the area between the ocean and the atmosphere where diffusion can take place, which leads to an enhanced gas transfer (Esters et al., 2018). The ocean is a significant carbon sink. Where turbulence takes place, the exchange of gases will be faster and the efficiency of the uptake of carbon dioxide, among others, will be increased (Tokoro et al., 2008). So, by gaining knowledge about turbulence, climate models can be improved to predict future climate scenarios.

Predicting turbulence in the ocean is difficult but important since measuring it is not straightforward. Various parameterizations on how to calculate surface turbulence have therefore been created. Three parameterizations are investigated in this thesis to see which one that describes the turbulence in the Baltic Sea best. The first one uses wind shear as a source of energy for turbulence and is called 'Law of the wall' (LOW) (Lorke & Peeters, 2006). The second one includes wind forcing that indirectly creates waves as well that contributes to the energy input to create turbulence, called $Terray$ in this thesis (Terray et al., 1996). The last one uses buoyancy-induced turbulence caused by convection and wind stress, called $B0$ in this thesis (Lombardo & Gregg, 1989).

1.1   Purpose

The purpose of this master thesis is to investigate the connection between the drivers of oceanic turbulence, for example wind, waves and buoyancy fluxes. The thesis will in particular study the enhanced turbulence events, which are defined as events when the oceanic turbulence exceeds the background levels.

1.2 Research questions

Four research questions were posed and investigated to reach this purpose:

- Which driving mechanisms is it that mainly creates the enhanced turbulence events?

- Does the wind direction correspond to the wave direction that we get from the ADCP?

- What kind of waves creates the enhanced turbulence events to greater extent? Long- or short-distance waves?

- Can existing turbulence parameterization explain the observations?

2 Background

2.1 Upper Ocean Turbulence

The upper 100 m of the ocean are called the ocean surface boundary layer (OSBL). The approximately 100 m is a mixed layer where temperature and salinity are nearly uniform with depth down to the pycnocline (Belcher et al., 2012). Within the OSBL there is a mixing layer that distinguishes from the mixed layer. The mixing layer is the layer that is being actively mixed by external sources at the surface at a given time. This depth zone usually corresponds to the same depth zone where there is enhanced turbulence as a result of surface forcing (Brainerd & Gregg, 1995). The turbulent motion that occurs in the OSBL controls the interaction between the ocean and the atmosphere that leads to the exchange of momentum, heat, and trace gases between them (Belcher et al., 2012).

Turbulence is a motion of a fluid that originates from the instability of laminar flow and occurs on many different scales, from global circulation down to microscale turbulence (Kantha & Clayson, 2000). The parameter that characterize the flow is the Reynolds number (Re). When a critical value of Re is exceeded the laminar flow will be replaced with a turbulent flow (Thorpe, 2007). Laminar and turbulent flows are a notion that describes the property of the flow and not the water (Hendriks, 2010). The mixing and dispersion of various particles in the ocean are a consequence of the turbulence that occurs on different scales. Turbulence also increases the area between the ocean and atmosphere where diffusion can take place and therefore enables an enhanced gas transfer in the air-sea interface (Esters et al., 2018). Turbulence is hard to describe and can not be said to be a property of a fluid, but can instead be seen as an energetic, rotation, and eddying state of motion (Thorpe, 2007).

2.2 Turbulent Kinetic Energy

Turbulence is generated as a result of the transfer of kinetic energy from different sources. There are three main sources of turbulence in the OSBL, wind, waves, and buoyancy that in return deepen the OSBL. The deepening of the OSBL is a consequence from an increase in potential energy where the energy is obtained from the turbulent kinetic energy (TKE) (Belcher et al., 2012).

The strength in turbulence can be said to be the TKE. It derives its energy from different sources. There are three terms that are the main contribution to the rate of change of the mean kinetic energy of the turbulent flow per unit volume. This can be described with the turbulent energy equation:

$$\frac{DE}{Dt} = P + B_0 - \epsilon \ , \tag{1}$$

where $\frac{DE}{Dt}$ is the mean rate of change of the TKE when it is carried by the mean flow, P is the rate of production by the mean flow, B_0 is the buoyancy flux and ϵ is the rate of dissipation. The terms in the equation are averages over a large volume or time. The turbulence is sustained if the terms in the equations are balanced, otherwise, the turbulence is growing or decaying (Thorpe, 2007).

One important property of turbulent flows is the viscous dissipation rate of TKE, ϵ. It is usually measured as the rate of dissipation of TKE per unit mass with the units of W/kg or m^2/s^3 (Thorpe, 2007). The dissipation rate describes the conversion of the kinetic energy of turbulent motion into thermal energy, in the form of heat, as a result of viscous forces (Fossum et al., 2013).

2.3   Turbulent spectrum - Energy Cascade

The concept of an energy cascade, when energy goes from macroscale to microscale was first introduced by *Richardson* in 1922 who also wrote a poem that gives a good overview of the phenomena:

> *Big whirls have little whirls that feed on their velocity,*
> *And little whirls have lesser whirls and so on to viscosity*
> *– in the molecular sense.*

The small eddies can be seen as a consequence of the motions of the larger eddies at the larger scales where the energy is supplied, introduced or produced. Here most of the kinetic energy is present. The energy is then passed down to smaller scales as a result of interactions or the instability between the eddies, and at this scale the inertial forces are dominant (Thorpe, 2007). At the smallest scale viscosity, which is an internal friction, dominates and the kinetic energy is dissipated into heat. For a flow to maintain its turbulence, new energy has to be supplied, which happens at the larger scales as mentioned earlier (Burchard & Umlauf, 2018).

Kolmogorov characterized the homogeneous isotropic turbulence in the early 1940s and suggested the phenomenon of an energy cascade where energy is introduced by external forces and then passed on to smaller scales as described above (McGillicuddy & Franks, 2019). The rate at which TKE is transferred from one scale to another is the same for all scales if the turbulence intensity does not change. From this, it follows that the rate of supplied TKE at the largest scale is the same as the rate of dissipation is at the smallest scales (Cushman, 2019). The created turbulence is characterized by two quantities, ϵ and the kinematic viscosity, ν. By looking at the dimensions of these quantities, which

is $L^2 T^{-3}$ for ϵ and $L^2 T^{-1}$ for ν, where L is length and T is time, it can be seen that the length scale for turbulent motions must be (Thorpe, 2007):

$$l_K = \left(\frac{\nu^3}{\epsilon}\right)^{1/4} .$$
(2)

Since turbulence is hard to describe and understand it is often simplified, so the nature of turbulence can be more easily understood. The simplification made is the assumption that the oceanic turbulence is isotropic. Isotropic turbulence means that the average properties at each point of the turbulence are independent of both position and direction and that the mean velocity is zero ($\overline{u'^2} = \overline{v'^2} = \overline{w'^2}$) (Glegg & Devenport, 2017). Under these conditions, ϵ can be described as:

$$\epsilon = \frac{15}{2}\nu\overline{(\frac{\partial u'}{\partial z})}^2 = 15\nu\overline{(\frac{\partial u'}{\partial x})}^2 ,$$
(3)

which describes the rate of the TKE cascade over the entire inertial subrange, where turbulence is only characterized by ν and ϵ. The inertial subrange lies between the source range, which consist of the energy containing eddies, and the dissipation range, where the eddies dissipates into heat due to the viscous forces, in the energy spectrum (Fig 1). Kolmogorov showed that if Re is very large and assuming homogeneous and isotropic turbulence in the inertial subrange, the theoretical spectrum only depends on ϵ. From this ϵ can then be calculated using the spectrum that is given by:

$$S(k) = q\epsilon^{2/3}k^{-5/3} ,$$
(4)

where q is an empirical constant and k is the wavenumber defined by $k = 2\pi/l$, where l is the size of the eddy. In the inertial subrange the slope, which is around -5/3, in the velocity spectrum remains almost constant (Thorpe, 2007).

In reality, turbulence is rarely isotropic and most turbulence flows are anisotropic especially at the macroscale. It is only at the microscale, in the inertial subrange and the dissipation range, that turbulence can partially be seen as isotropic (Kantha &, Clayson 2000).
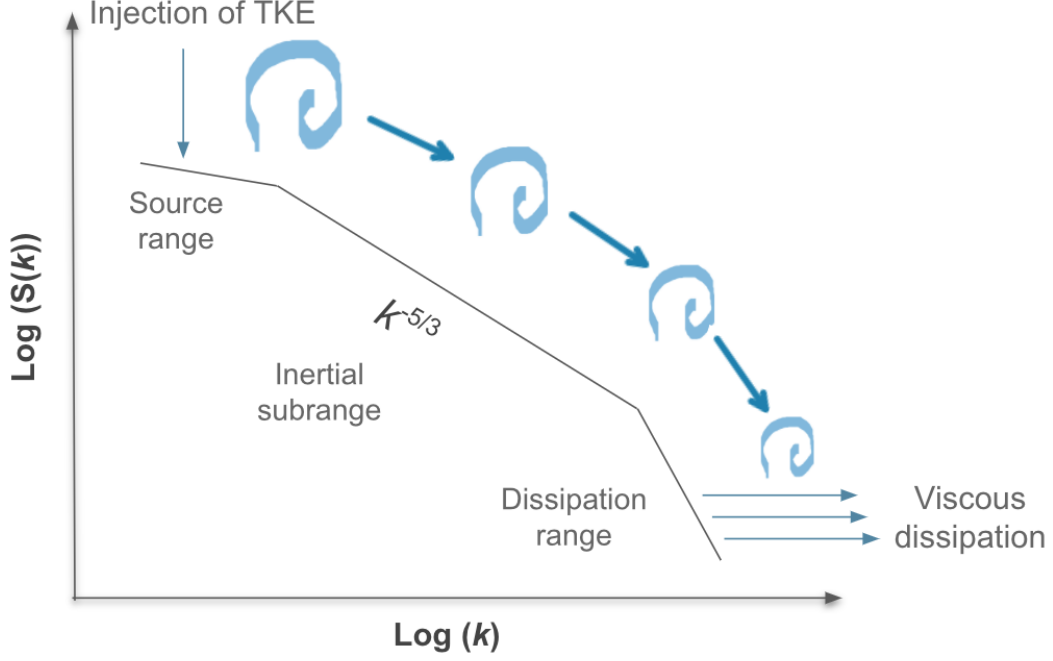
Injection of TKE

Source range

$k^{-5/3}$

Inertial subrange

Dissipation range

Viscous dissipation

Log (S(k))

Log (k)

Figure 1: The Kolmogorov energy spectrum of the turbulent velocity cascade. S(k) is the spectral density and k is the wavenumber. Kinetic energy is injected in the source range and cascades through the inertial subrange down to the dissipation range where viscose forces dissipate the energy into heat (Ryden, 2009).

2.4 Driving mechanism for Oceanic Turbulence

This project is focused on the external driving mechanism that affect the rate of turbulence in the OSBL. The generation of turbulence in the OSBL is due to the air-sea interactions where there is an exchange of heat, freshwater fluxes, gases and momentum through wind stress (Esters et al. 2018).

In this section different approaches on how to describe and parametrize oceanic turbulence will be introduced depending on what drivers of turbulence that are considered.

2.4.1 Shear driven Turbulence - The Law of the Wall

In the absence of breaking surface waves as drivers of turbulence, the OSBL can be seen as a flat rigid 'wall'. During these conditions the turbulence and mean flow is steady. This means that in Equation (1) $DE/Dt = 0$ and the buoyancy flux is negligible. It remains then the balance between the two other terms, the rate of production of TKE as a result of wind shear and ϵ (Thorpe, 2007). The constant stress that is produced by wind on the surface layer results in a shear that is given by:

$$\frac{dU}{dz} = \frac{u_{*w}}{\kappa z} \, , \tag{5}$$

where $\kappa \approx 0.41$ is the von Karman constant and dU/dz is the mean velocity shear, which is scaled by $u_{*w}=$ water-side friction velocity and $z=$distance from the boundary (Kantha & Clayson, 2000).

In the turbulent OSBL the turbulence usually increases towards the interface. During these conditions, ϵ is inversely proportional to z. This results in the scaling that is referred to as the 'Law of the wall' (LOW) (Lorke & Peeters, 2006):

$$\epsilon_{LOW}(z) = \frac{u_{*w}^3}{\kappa z} \ .$$

(6)

This is a parameterization that is applicable if the shear caused by wind stress is the only driver of turbulence, which usually is not the case. In addition to shear stress caused by wind, the turbulence is also affected by two other main sources, waves and buoyancy (Belcher et al., 2012).

2.4.2 Wind-Wave Induced Turbulence

The first term in Equation (1) refers to two of the main sources that produce TKE in the OSBL, wind and waves. Wind-forced production of TKE in the upper ocean is believed to be generated both through direct action of wind stress on the ocean surface and through an indirect process of creating surface waves as a result of the forcing on the surface (Gargett & Grosch, 2014).

Formation of waves depends on three parameters, wind speed, fetch length and the amount of time the wind blows consistently over the fetch. The wind fetch is determined by the distance over water that the wind blows with similar speed and direction. A long distance and higher wind speeds for long time periods will result in the highest waves. If the waves on the other hand are a direct consequence of the local wind they will be short, choppy, and usually break at wind speeds around 6 m/s (Ainsworth, 2018). The threshold of 6 m/s for breaking waves can also be argued to be used by reading an article by *Scalon & Ward* (2016). They mean that this wind speed is within the range where the parameterization for whitecapping (breaking waves) starts to diverge.

A measurement used to report the wave height is the significant wave height, H_s. This parameter is defined as the average height of the highest 1/3 waves in a wave spectrum. The definition corresponds to what a mariner observes when estimating the wave height. Therefore H_s does not respond to the height of the most frequent wave height. The mean wave height is approximately around 2/3rds of the value of H_s and the maximum wave height is approximately two times the value of H_s (Ainsworth, 2018).

The momentum from wind gets transferred to the wave field via wave breaking at moderate to high wind speeds. Dissipation of wave energy is caused by the breaking of surface waves and this is why this is seen as a source of enhanced TKE in the near-surface layer (Gemmrich & Farmer, 2004). The importance of surface waves and mixing of the upper-ocean was also shown by *Wu et al* (2015). The cause for the mixing was due to four main processes which included wave-breaking and stirring by non-breaking waves. The non-breaking waves are more important under low-wind conditions than during high-wind conditions but it was shown that the non-breaking waves demonstrate a considerable impact on the upper-ocean mixing and give better model results when included (Wu et al., 2015).

To account for the fact that wind does not only cause turbulence as a result of shear drag, but also wave breaking *Terray et al.* (1996) introduced a parameterization. This param-

eterization is appropriate to use during conditions when the wind is rough enough so the stress is communicated to waves, there are waves breaking and the observations are done within a few wave heights of the surface. They found that during these conditions ϵ can be scaled with the energy flux from the wind momentum that is transferred into the waves.

The enhanced turbulence caused by breaking waves has an impact on the shallow layer at the surface with a depth in the order of H_s. This layer is then divided into three sublayers. The top layer, called the breaking zone, is where turbulence is injected from the breaking waves. The depth of this zone, z_b, is estimated to be $0.6H_s$ and the dissipation rate here, ϵ_b, is assumed to be constant from the surface down to z_b. To calculate this dissipation rate the following equation is used (Terray et al., 1996):

$$\frac{\epsilon H_s}{u_{*w}^2 \overline{c}} = 0.3 \left(\frac{z_b}{H_s} \right)^{-2} . \tag{7}$$

The layer in the middle, the transition layer, is where the TKE is transported downward by turbulence from the breaking layer while it simultaneously is dissipated. Here the dissipation rate is decaying with depth as z^{-2} and the depth, z_t, can be expressed by:

$$\frac{z_t}{H_s} = 0.3 \frac{\kappa \overline{c}}{u_{*w}} , \tag{8}$$

where $\overline{c}$ is the effective phase speed for the wind. The wind stress, τ_a, and $\overline{c}$ can together give a parameterization of the wind input:

$$F \equiv \frac{\tau_a \overline{c}}{\rho_w} \approx u_{*w}^2 \overline{c} , \tag{9}$$

where τ_a, is the surface values of the turbulent stress and has been approximated to have the following equality:

$$\tau_a \equiv \rho_a u_{*a}^2 \approx \rho_w u_{*w}^2 , \tag{10}$$

here ρ_a and ρ_w are the air- and water-side densities and u_{*a} are the air-side friction velocity (Terray et al., 1996).

The transition layer is finally merged into the wall layer that can be described by the 'Law of the wall' scaling described in Section 2.4.1 where the local shear production dominate the generation of turbulence (Terray et al., 1996).

A conclusion to how *Terray et al.* (1996) scaled ϵ in a wind-forced surface-layer with different layers is the following:

$$\epsilon_{Terray} = \begin{cases} 0.3 \frac{u_{*w}^2 \overline{c}}{H_s} \left(\frac{z_b}{H_s} \right)^{-2} & \text{above } z_b \\ 0.3 \frac{u_{*w}^2 \overline{c}}{H_s} \left(\frac{|z|}{H_s} \right)^{-2} & \text{between } z_b \text{ and } z_t \\ \frac{u_{*w}^3}{\kappa z} & \text{below } z_t \end{cases} . \tag{11}$$

2.4.3 Buoyancy Induced Turbulence

The second term in the turbulent energy equation (Eq. 1),B_0, is the one connected to the generation of buoyancy-induced turbulence. Much of the induced turbulence in the OSBL

can be identified as external processes and one of these is the convection that is caused by the air-sea buoyancy flux. This is a result of the interaction between the atmosphere and the ocean. Buoyancy flux has direct effects on the mixing of the boundary layer and is often dominated by a flux of heat (Thorpe, 2007).

The mixing of the surface layers is connected to the diurnal day-night cycle of heating and cooling. So it is essential to study the warming and stratification that occurs during the day and the cooling and mixing during the night which results in the cycle of turbulent motion. The net effect of these two phases controls the average sea surface temperature, which in return is significant for the oceanic feedback to the atmosphere. The phases also affect one another and are therefore coupled. The convective deepening that occurs during night affects the initial state of the turbulence during the day, and the stratification established during the day affects the rate of the deepening of the mixed layer during the night (Brainerd & Gregg, 1993).

The surface buoyancy flux is a result of many different parameters and can be calculated using the following equation:

$$B_0 = \frac{g}{\rho} \left(\frac{\alpha \cdot Q_0}{c_p} + \frac{SA \cdot \beta \cdot LE}{(1 - SA)H} \right) \ , \tag{12}$$

where g is the gravity force [m/s], ρ is the density of the surface water [kg/m^3], Q_0 is the net heat flux at the surface [W/m^2], c_p is the specific heat of water at constant pressure [J/kg K], SA is the absolute salinity [g/kg], LE is the latent heat flux [J/kg], H is the latent heat of evaporation [J/kg]. α and β are calculated with the following equations:

$$\alpha \equiv -\rho^{-1} \frac{\partial \rho}{\partial T} \ , \tag{13}$$

$$\beta \equiv \rho^{-1} \frac{\partial \rho}{\partial S} \ , \tag{14}$$

where α is the thermal expansion coefficient [$^\circ$C^{-1}], β is the saline contraction coefficient [g/kg], T is the surface water temperature [$^\circ$C] and S is the surface salinity [g/kg] (Brainerd & Gregg, 1993).

Buoyancy fluxes as a source of turbulence dominate when the stress is negligible, thus there is no wind. The motion of buoyancy-induced turbulence comes from unstable stratification and convection. But it is more common that there are both buoyancy and momentum fluxes that generate turbulence (Thorpe, 2007). *Lombardo & Gregg* (1989) showed a similarity scaling for this situation, when both wind stress and buoyancy enhances the turbulence:

$$\epsilon_{B0} = 0.87 \left(1.76 \epsilon_{LOW} + 0.58 B_0 \right) \ . \tag{15}$$

In this scaling they have added the influence of buoyancy fluxes as a source of turbulence to the LOW scaling. B_0 is calculated using the equation from *Brainerd & Gregg* (1993) (Eq. 12) and the buoyancy flux is defined as positive into the ocean.

3 Data Acquisition

3.1 Measurement sites

For this project, one measurement site was used that includes instruments, which are mounted at four different positions that represent the same characteristics for atmospheric and oceanic parameters. This measurement site is located on the island Östergarnsholm situated in the Baltic Sea, 57.43010 N 18.98415 E. Östergarnsholm is situated about 4 km east of the coast of Gotland. The island is flat with little vegetation and stretches around 2 km in W-E and N-S direction respectively (ICOS, n.d.). The air-side measurements on the island are conducted from the southern tip of the island. The measurements are conducted from a 30 m tall tower situated around 1 m over sea level, where the wind speed and direction is measured at 12 m. For the turbulent measurement at the tower, high-frequency instrumentation is used. The high-frequency wind components are measured with CSAT3-3D sonic anemometers (Rutgersson et al., 2020).

Not all of the components in the total radiation flux was measured at the measurement site of Östergarnsholm. Due to this, the the net short- and longwave radiation was downloaded from the NCEP/NCAR Reanalysis. The extracted data is from the closet position of Östergarnsholm in 2020 with 4 values per day (NOAA, 1994).

The oceanic data was collected from three different sites. One site is situated next to the island at around 1 m depth and measure the surface salinity and surface water temperature with a HOBO-sensor. The second one is located 4 km southeast of Östergarnsholm. Wave data, like H_s and wave direction, from a directional waverider moored at a depth of 39 m is collected here, operated by the Finnish Meteorological Institute (ICOS, n.d.). The third measurement site is located around 1 km southeast of the tips of Östergarnsholm. Here the Acoustic Doppler Current Profiler (ADCP) is situated at the bottom of the ocean at around 20 m under sea level. The ADCP gives data for the waves, currents and the turbulence. These three sites can be seen in Fig. (2).
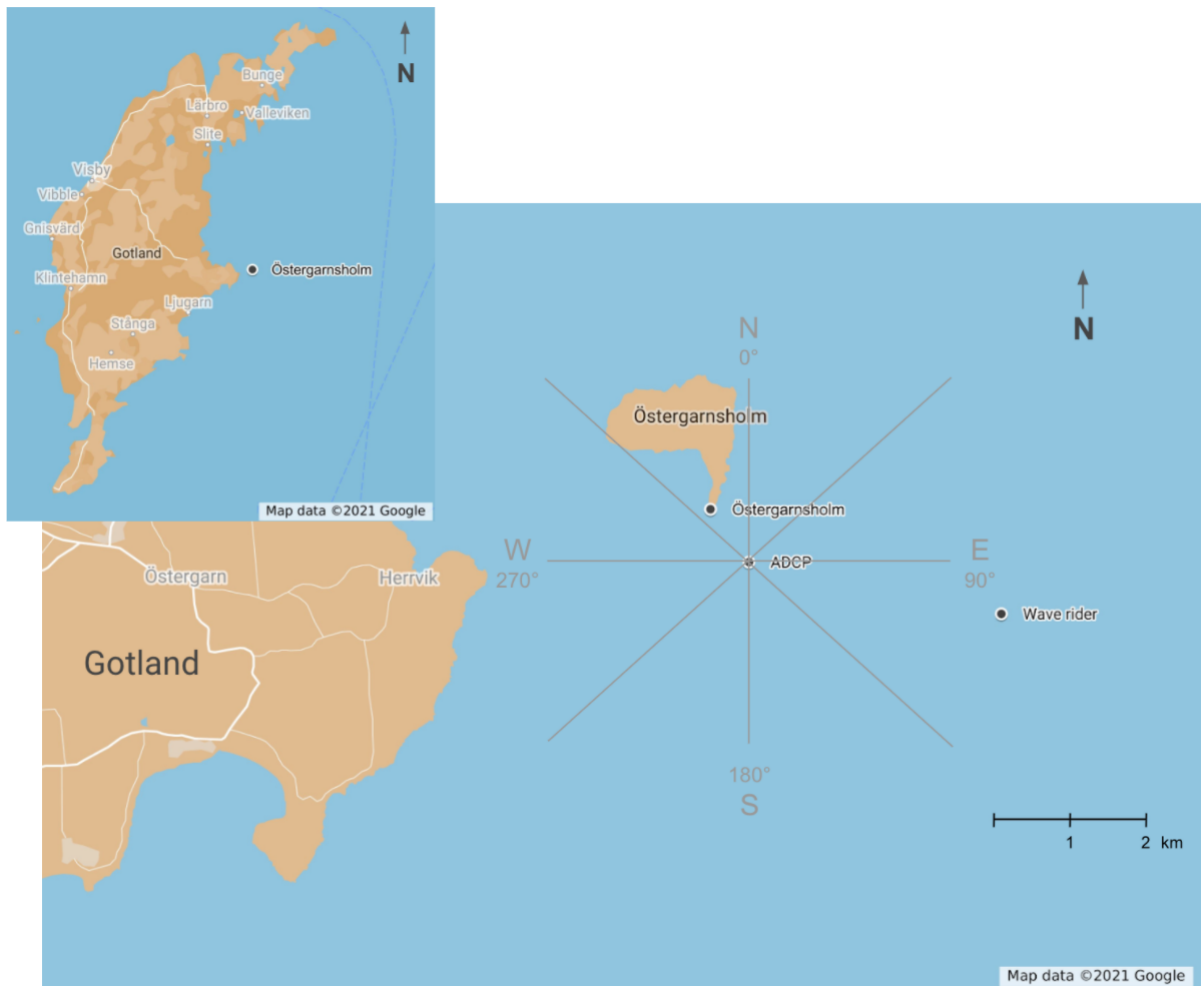
Figure 2: Map showing the positions of the measurement sites and where they are located in relation to Gotland. The position of the ADCP also shows the degree of directions. (Google maps, n.d.)

3.2 Data

The focus of this thesis is on the data collected by the ADCP that was deployed in May 2020. It was deployed for almost 6 months and collected data until mid October. The analysis includes studying and comparing the turbulence with meteorological parameters. All the parameters that were used either in a comparison or in any calculation is stated below in Table (1).

Table 1: Table showing all of the parameters that were used in the analysis.

Variable	Measurement site	Time averages
Wind speed (12 m)	Östergarnsholm	30 min
Wind direction (12 m)	Östergarnsholm	30 min
Kinematic sensible heat flux (10 m)	Östergarnsholm	30 min
Kinematic latent heat flux (10 m)	Östergarnsholm	30 min
Air-side friction velocity (10 m)	Östergarnsholm	30 min
Relative humidity	Östergarnsholm	30 min
Air temperature	Östergarnsholm	30 min
Air pressure	Östergarnsholm	30 min
Surface salinity	HOBO-sensor	1 h
Surface water temperature	HOBO-sensor	1 h
Net longwave radiation	NCEP/NCAR	4 times/day
Net shortwave radiation	NCEP/NCAR	4 times/day
H_s	Wave rider	30 min
Wave direction	Wave rider	30 min
H_s	ADCP	10 min averages (with exceptions)
Wave direction	ADCP	10 min averages (with exceptions)
Wave period	ADCP	10 min averages (with exceptions)

To get the water-side friction velocity, the air-side friction velocity was used by using the law of momentum conservation (Eq. 10).

3.2.1 ADCP

To obtain information about the movement in the water, like waves, currents and turbulence, an ADCP was used. To receive this information the ADCP uses sound waves, sent out at a known frequency, that travels up through the water column from five narrow beams pointed in different directions. One beam is positioned in the middle and is vertical. This beam is the one that measures the sound speed from which the turbulence is estimated and is calculated for bins of 0.5 m. The other four beams are positioned at the same angle to the vertical. The vertical beam is measuring the turbulence at a frequency of 8 Hz, which allows for estimating the turbulence.

To measure the current speed, the sound wave sent by the ADCP will be reflected of suspended particles in the water column and return to the ADCP, with a changed frequency as a result of the moving particles. This frequency shift is due to the Doppler effect, and from this the movement of the particles and the movement of the water can be calculated (Alderton & Elias, 2021). It takes longer for the sound waves to hit particles further away from the ADCP than close. By knowing the speed of sound in seawater, the ADCP can measure at many different depths (Thorpe, 2007).

To determine ϵ, and therefore getting an idea on the level of turbulence, the ADCP uses the spectrum showed in Eq. (4). To estimate the turbulence in form of ϵ ,Taylor's frozen

field hypothesis is used, that suggests that the eddies are frozen while they are advected past a fixed point, meaning that the properties does not change. The spectrum is then transformed to a frequency spectrum $S(f)$:

$$S(f) = \left(\frac{U}{2\pi}\right)^{2/3} q\epsilon^{2/3} f^{-5/3} \quad, \tag{16}$$

where U is the mean velocity of the flow [m/s] and f is the frequency [1/s]. By solving for ϵ we get the following equation:

$$\epsilon = \frac{2\pi}{U} q^{-3/2} \left[f^{5/3} S(f)\right]^{3/2} \quad, \tag{17}$$

where the averaging in the inertial subrange is described by the squared brackets. The spectrum is then interpolated smoothed for reducing the scatter so it gets easier to detect the slope at -5/3 so the inertial subrange can be identified. On top of this, the noise level is also determined for each spectrum and then subtracted. The slope is detected based on linear fitting of the data with a threshold of 0.3. This is as much as the detected slope is allowed to differ from the theoretical slope at -5/3.

4 Method

4.1 Driving mechanisms for the generation of enhanced turbulence events

Initially, the time periods during which enhanced turbulence events occur were chosen. A limited time period was chosen because of the limitations in data, from missing data for parameters for the buoyancy calculations, and investigating the whole time period between May and October would be too time-consuming.

Since the most positive buoyancy data was found during June-August (Appendix A.1), the wind data for this period was investigated for increased wind speeds. This was conducted by studying Fig. (3) and four time periods were selected for further investigation (Table 2).
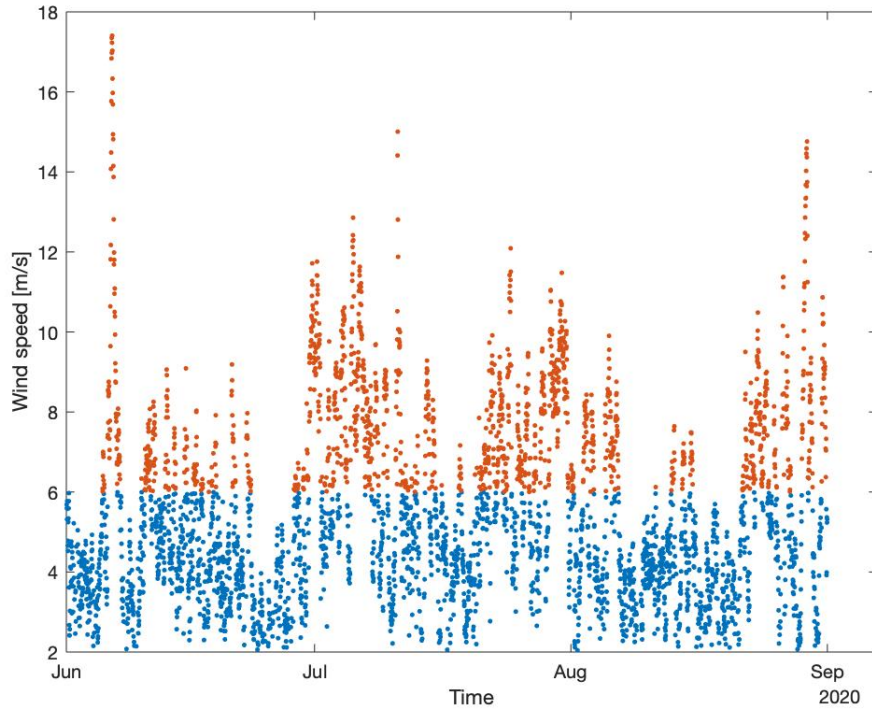
Figure 3: Wind speeds June to August. The orange points show when the wind speeds exceed 6 m/s.

For the four chosen time periods, the turbulence data were compared to the wind speed (WS) and H_s. The turbulence data is shown as the depth of the mixing layer. This is the depth at which ϵ has fallen to a value of 10^{-4} m^{2}s^{-3}. This parameter is hereafter called $xld4m$. The $xld4m$ will be used as an indication for the level of turbulence. When turbulence increases and enhanced turbulence reaches to deeper depths, the $xld4m$ will be deepened.

Correlation coefficients were calculated for WS vs. $xld4m$ (R_{WS}) and H_s vs. $xld4m$ (R_{Hs}) to see how they corresponded to each other. Since the four chosen time periods stretches over several days these periods were divided into sub-periods to give more accurate correlation coefficients and to make the overall analysis of the enhanced turbulence events easier. The division of the four periods into sub-periods was conducted by studying the line for $xld4m$ and see where it decreased, meaning that the turbulence was lower than its surroundings. Table 2 shows the sub-periods.

Table 2: Dates of the chosen periods and sub-periods.

Period	Date	Sub-period	Date
1	June 5-7	1	5/6 00:00 - 6/6 00:00
		2	6/6 00:00 - 7/6 00:00
2	July 1-11	1	1/7 00:00 - 2/7 12:00
		2	2/7 12:00 - 3/7 19:00
		3	3/7 19:00 - 5/7 15:00
		4	5/7 15:00 - 8/7 02:00
		5	8/7 02:00 - 10/7 06:00
		6	10/7 06:00 - 11/7 04:00
3	July 23 - August 05	1	23/7 23:00 - 25/7 01:00
		2	25/7 01:00 - 27/7 10:00
		3	30/7 07:00 - 31/7 10:00
		4	31/7 10:00 - 02/8 11:30
		5	02/8 11:30 - 04/8 03:00
		6	04/8 03:00 - 05/8 15:00
4	August 22-30	1	22/8 00:00 - 22/8 12:00
		2	22/8 12:00 - 23/8 15:00
		3	23/8 15:00 - 25/8 13:00
		4	25/8 13:00 - 28/8 13:00
		5	28/8 13:00 - 30/8 11:00

Additionally, the mean WS, $\overline{WS}$, the mean H_s, $\overline{H_s}$, and the standard deviation for WS and H_s, σ_{WS} and σ_{Hs} were calculated.

In order to investigate the potential impact of buoyancy, the buoyancy was calculated using Eq. (12). The data of the salinity, that was needed for the calculation, was not complete so missing values were replaced with the total mean, sal_{mean}. This was possible to conduct due to the fact that the exact value of salinity does not change the buoyancy calculations in a significant way. The buoyancy could not be calculated for all points in time since some data were missing. It was found that where there were most positive buoyancy values in the chosen time period from June to August but here, the turbulence data were missing due to saving errors while the ADCP collected the data. Why positive values were desirable was because this is when convection is occurring that leads to turbulence at the surface.

4.2 Direction of Wind and Waves

The wind and wave distribution was investigated to receive an overview on the wind speed and direction and the wave height and direction. The wind data was limited to when wave data were available. This was completed by finding the points in time in the

wind data that corresponded to the time for the wave data. By doing this the amount of data was the same for both.

In addition, the relation between wind and wave direction and the direction for waves from the ADCP and from the Wave rider was investigated.

Last, the mean wind direction and mean wave direction with a percentage on how well the wave direction corresponded to the wind direction was calculated for each sub-period. The percentage show the wave direction divided by the wind direction multiplied with 100.

4.3 Wave-induced turbulence

The direction for long- and short-distance waves were defined by studying Fig. (2). This map points out the location for the ADCP and the directions. The long-distance waves come from the open ocean and are not affected by Östergarnsholm or Gotland, while the short distance waves come from the shorelines of these coasts.

In the events where it looks like the waves follow the turbulence it was investigated if it was caused by long- or short-distance waves.

4.4 Parameterization

According to the parameterization described in Section 2.4, different parameterizations can be used to calculate the turbulence. This was used to make a comparison to the measured turbulence for the different periods described in Table (2).

First, the turbulence was calculated using the different equations for the parameterizations. The three different scenarios were:

- Shear driven Turbulence, LOW: Eq. (6)

- Wind-Wave Induced Turbulence, Terray: Eq. (11)

- Buoyancy Induced Turbulence, B0: Eq. (15)

The results was then averaged over the sub-periods over the depth.

To see if the parameterization over-predicted or under-predicted the measured turbulence, the measured turbulence was divided by the calculated parameterized turbulence. An averaged value for each depth was then calculated. This was conducted for all sub-periods.

To get a number on how well the parameterization is correlated and follows the measured turbulence the correlation coefficient between the measured turbulence, eps, and the parameterized turbulence, $Terray$ and LOW, was conducted. The correlation coefficient was calculated for the upper 5 m since the focus lies on the turbulence connected to the atmosphere in this thesis. This was not conducted for the B0 parameterization since there was too much missing data, which could lead to misleading results. In addition, the

difference between *eps* and the parameterization, $Terray$ and LOW, was calculated by subtracting the mean value of $Terray$ and LOW from the mean value of *eps* for each sub-periods, also for only the upper 5 m instead of the whole water column. An average for the difference was then calculated for each sub-period for the two parameterizations. By doing this it could be seen how large the difference was between the measured turbulence and the calculated turbulence and a value was presented for each sub-period, called Diff_{Terray} and Diff_{LOW}. A smaller difference shows that the parameterization is closer to the real measured turbulence. To supplement this, a percentage for the difference was also calculated. This was conducted by taking the calculated difference and dividing it with the measured turbulence.

5 Results

5.1 Driving mechanisms for generation of enhanced turbulence events

How the turbulence varied during the four chosen time periods can be seen in Fig. (4). Here the turbulence is illustrated from the surface down to 0.5 m above the ADCP. The figures includes a black line that illustrates $xld4m$, which shows when the logarithmic ϵ is 10^{-4} m^{2}s^{-3}. It can be seen that in all four periods that the turbulence is higher at the surface, and decreases further down. But in some cases, like in the beginning of period 1, there is more turbulence further down, not connected to the surface. This can be seen in more periods as well but in smaller scale.
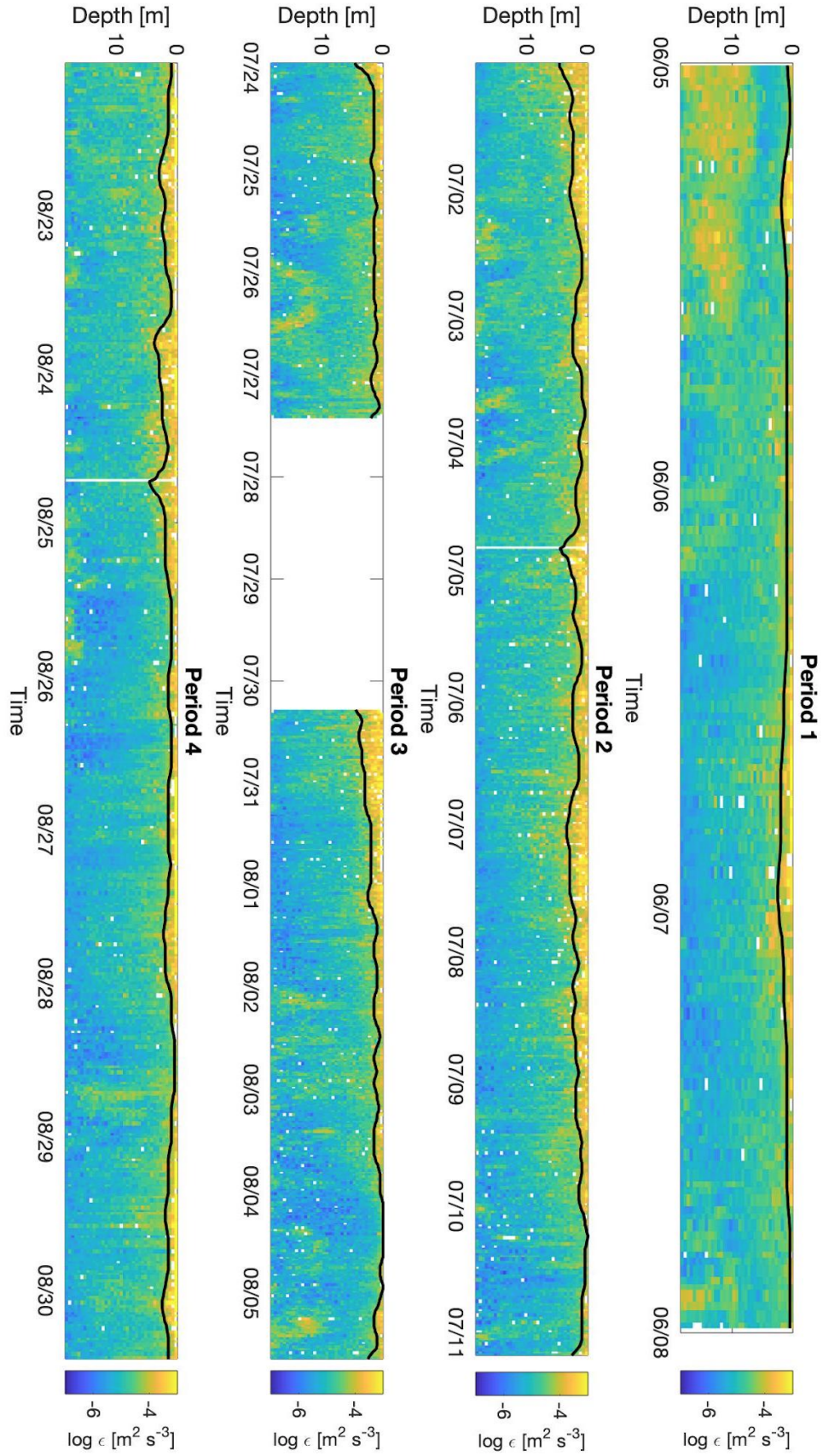
Figure 4: Turbulence over the water column, surface down to 0.5 m over the ADCP. The colors shows the level of $\log(\epsilon)$ is. The black line shows $xld4m$, that shows the depth to which active turbulence reaches.

17

Table (3) shows R_{WS}, R_{Hs}, the mean wind speed ($\overline{WS}$), the mean H_s ($\overline{H_s}$) and the standard deviation for WS and H_s for the different sub-periods. The sub-periods that are highlighted in purple show when the correlation coefficient is higher or equal to 0.5 for both cases. The sub-periods highlighted in yellow show the sub-periods that have a higher or equal value to 0.5 for R_{Hs} and the blue highlighted sub-period show when R_{WS} is higher or equal to 0.5. It can be seen that among the highlighted sub-periods, there are more times when both cases have a higher value than 0.5 than just one of them. This occurs 5 times while it happens 4 times for the R_{Hs} case and 1 time for the R_{WS} case.

By comparing the sub-periods that are highlighted in purple to Fig. (5) and (6), it can be seen how WS, $xld4m$ and H_s are behaving in comparison to each other. For P1:2, an increase in H_s can be seen where WS has a peak. The $xld4m$ shows the same peak but is delayed around half a day. In P2:6 it can be seen that both $xld4m$ and H_s are increasing as the WS is increasing, but they do increase steady without any distinct peaks, unlike WS. For period 3 both P3:5 and P3:6 show the same peaks in $xld4m$ as is seen for WS. The H_s show an increase when there is an increase in WS for both cases as well. In P4:5 it can be seen that H_s has a peak at the first peak in WS, but are thereafter decreasing even though there is a second peak in WS. There is also an increase in $xld4m$ where there are peaks in WS, but more for the second peak that has a lower WS and no increase in H_s.

Table 3: Table of correlation coefficients (R_{WS} and R_{Hs}), mean WS and H_s and standard deviation for WS and H_S. The blue highlight show when $R_{WS} \geq 0.5$. The yellow highlight show when $R_{Hs} \geq 0.5$. The purple highlight show when both cases have a correlation coefficient ≥ 0.5.

Period	Sub-period	R_{WS}	$\overline{WS}$ [m/s]	σ_{WS}	R_{Hs}	$\overline{H_s}$ [m]	σ_{Hs}	#obs.
1	1	0.50	4.96	1.00	0.19	0.15	0.019	48
	2	0.53	8.71	3.97	0.51	0.94	0.56	96
2	1	0.48	7.21	2.53	0.59	0.78	0.28	73
	2	-0.75	6.99	1.51	-0.40	0.63	0.097	61
	3	-0.24	7.34	2.28	0.21	0.83	0.22	88
	4	-0.46	8.25	1.93	-0.57	1.01	0.25	119
	5	0.11	6.05	1.99	0.51	0.59	0.18	103
	6	0.62	6.02	3.59	0.63	0.42	0.16	45
3	1	-0.36	7.16	2.45	-0.45	0.84	0.32	53
	2	-0.14	6.07	1.57	0.0079	0.56	0.16	115
	3	0.022	9.19	0.94	0.38	0.80	0.078	55
	4	0.48	5.08	1.75	0.76	0.42	0.16	99
	5	0.74	6.10	1.71	0.69	0.51	0.19	79
	6	0.70	5.03	2.18	0.79	0.27	0.19	73
4	1	-0.48	5.91	1.84	0.70	0.71	0.064	23
	2	-0.32	6.80	1.78	0.16	0.69	0.14	54
	3	-0.044	6.97	1.43	0.36	0.63	0.17	93
	4	-0.051	5.51	2.12	0.46	0.79	0.44	144
	5	0.56	7.62	3.61	0.51	1.04	0.77	92

An overview of how $xld4m$ changes over the four different periods compared to WS and H_s is shown in Fig. (5). Here the periods are also divided into its sub-periods. The sub-periods were divided from studying Fig. (5) to find where $xld4m$ decreased to see where a appropriate cut-off would be.
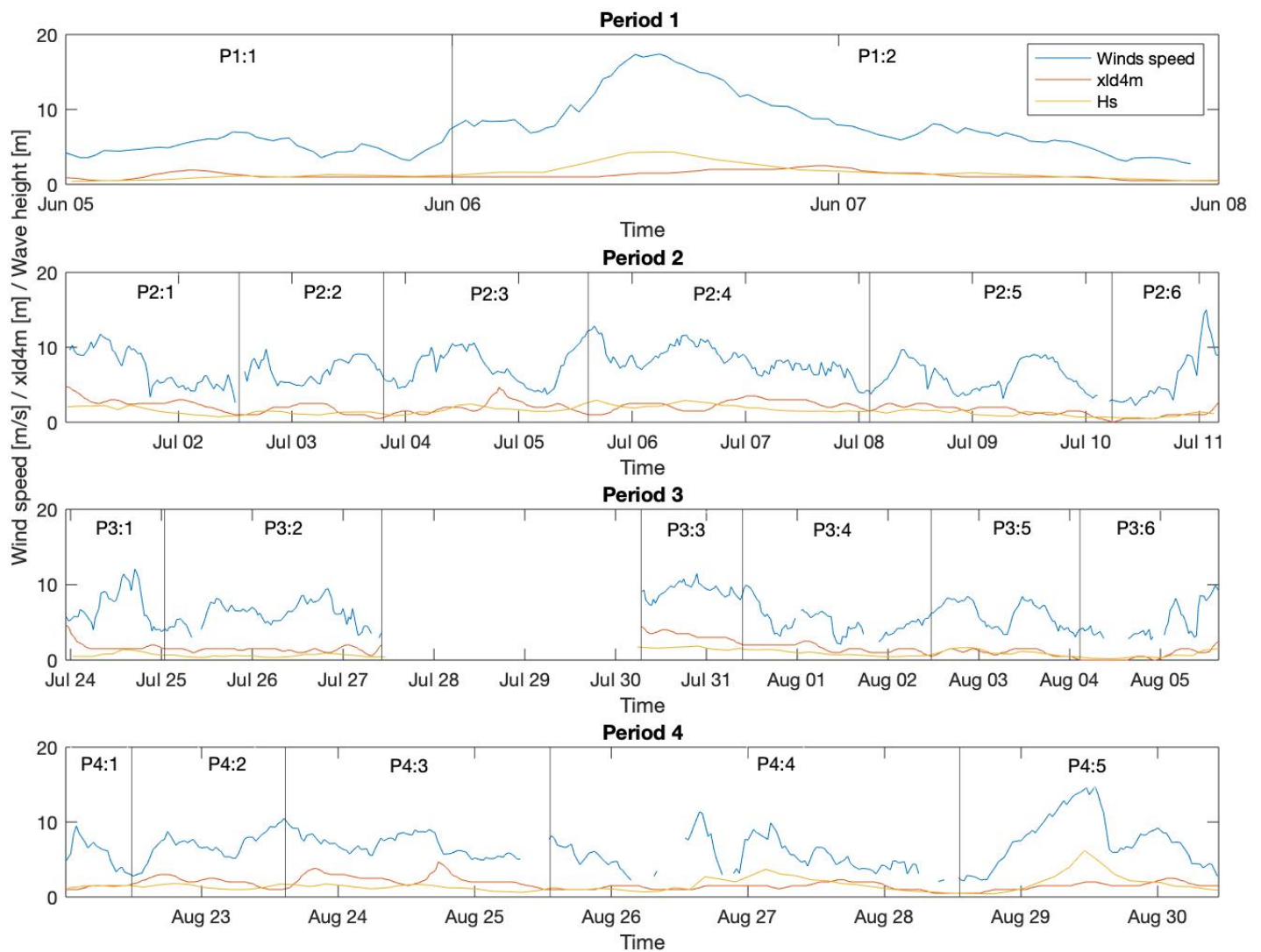

Figure 5: An overview on how WS, $xld4m$ and H_s varies during the chosen time periods. The blue line shows WS, the orange line shows $xld4m$, and the yellow line shows H_s multiplied by 2 to show the variations better.
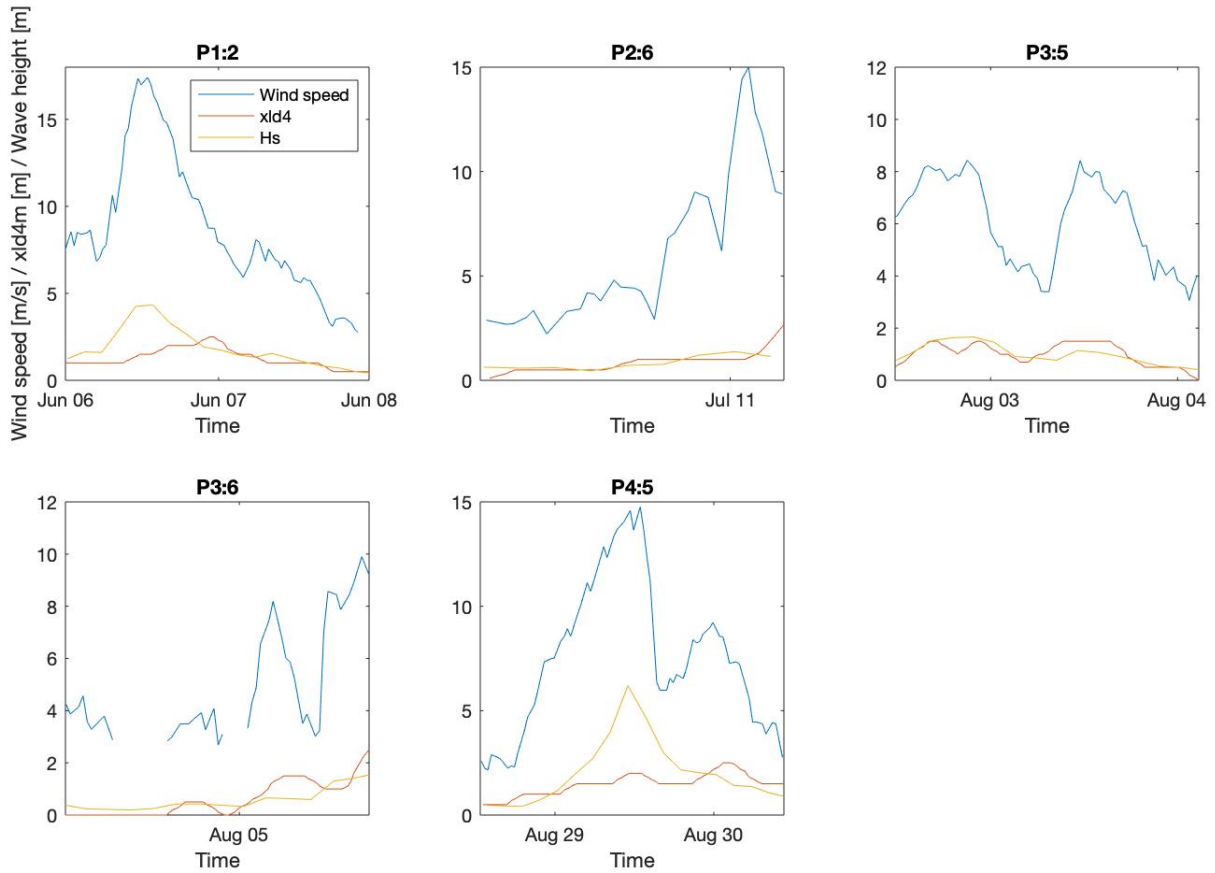
Figure 6: Variations for WS, H_s and $xld4m$ for the chosen five sub-periods that showed the best correlation coefficient in Table (3). The yellow line, that shows H_s is multiplied with a factor of 2 to more easily show the variations. The blue line shows WS and the orange line shows $xld4m$.

5.2 Direction of Wind and Waves

By studying the wind and wave roses (Fig. 7) it can be seen that the Wave rider measures waves that come from up to 210° while the ADCP measures waves from directions only up to 190°. The amount of waves from the different locations looks to be shifted to the right for the ADCP compared to the Wave rider. Other than this the size of the H_s, illustrated by different colors, differs for the two roses. The wave rider shows larger values of H_s compared to the ADCP. The wind rose that shows the wind distribution shows wind coming from all directions except where the wind is affected by the island Östergarnsholm and has been excluded from the data. The most frequent wind direction appears to be 190° - 210°, which is the same for the wave direction for the Wave rider. The ADCP does not have any waves for this direction but the main direction of the waves have the appearance to be shifted to 170° - 190° instead.
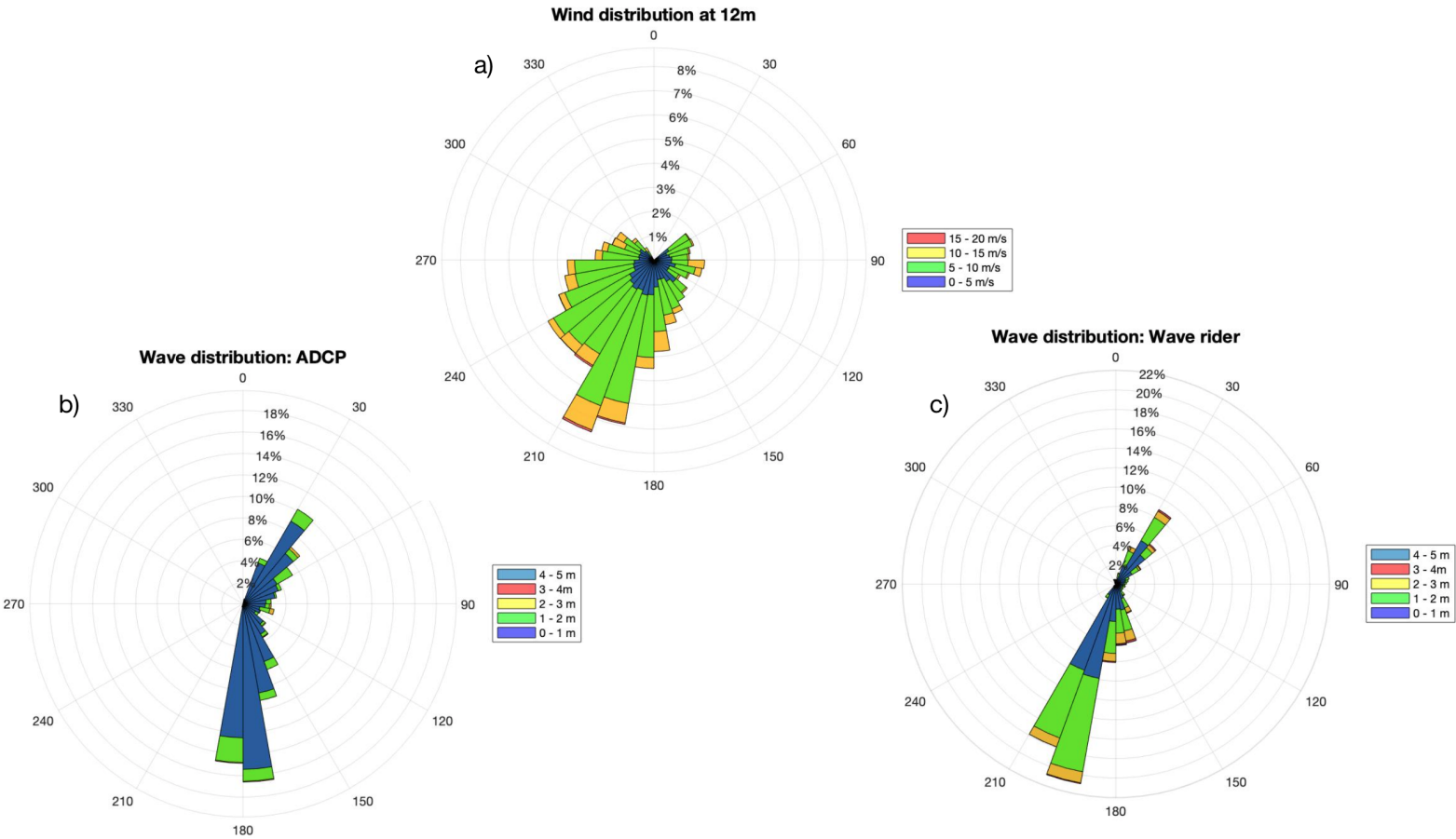
Figure 7: Wind and wave roses that show the distribution of the direction, strength and size for wind and significant waves, see inserted color bar. a) the wind rose, with wind data from the island of Östergarnsholm, b) wave rose with wave data from the ADCP, c) wave rose with wave data from the Wave rider.

The scatter plots generated with the associated coefficient of determination can be seen in Fig. (8). Fig. 8a) shows the correlation between the wave direction from the ADCP and the wind direction. It has a R^2-value of 0.18 with the points scattered all over. But it can be detected that at around 150° - 190° for the ADCP and around 170° - 270° for the wind most of the points are gathered. This means that most of the wind and waves come from this direction. In addition, the highest H_s occur when the wind and waves come from around 100°. But there are a few points with even higher significant wave height at around 150° for the wave direction and at around 130° for the wind direction.

Fig. 8b) shows the correlation between the wave direction from the Wave rider and the wind direction. Here the R^2-value, 0.05, is lower than for Fig. 8a). Most points are located around 160° - 210° for the wave direction and 170° - 270° for the wind direction. The highest H_s also seems to come from around 150° for the wave direction and around 130° for the wind direction, like for Fig. 8a).

Fig. 8c) shows the correlation between the direction of waves from the ADCP and the Wave rider. It has a R^2-value of 0.73, which says that that the correlation between the wave direction of the two locations have similarities but that there still are some differences. This can also be seen by studying Fig. 8c) where points are scattered and do

21

not follow a 1-to-1 line in the middle at all time. Further it can be seen that the highest H_s are around 150° for the wave direction, both for the ADCP and the Wave rider.
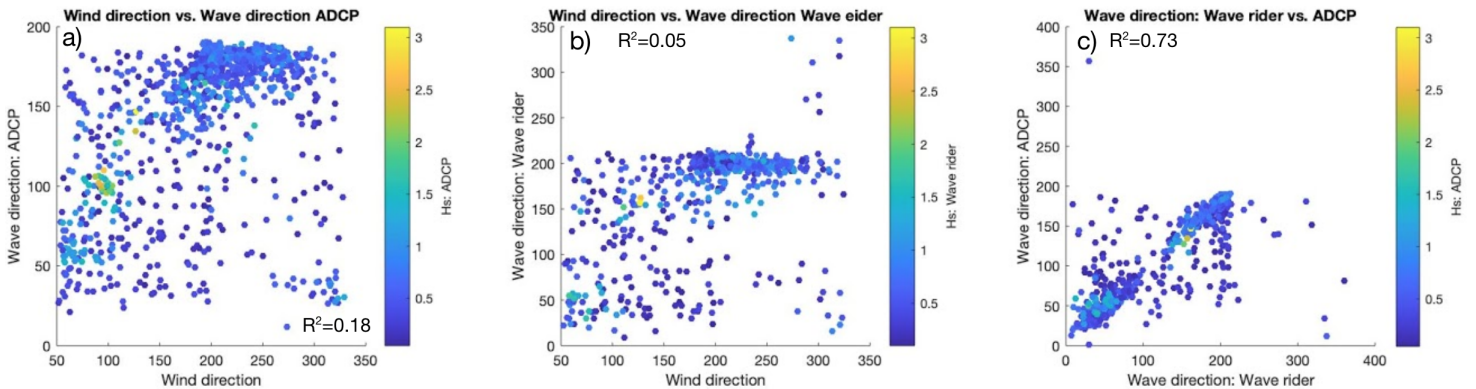

Figure 8: Scatterplots between a) the wind direction and wave direction for the ADCP, b) the wind direction and wave direction from the Wave rider and c) the wave direction for the ADCP and the Wave rider. The colour code shows the significant wave height, H_s.

The difference between the mean wind direction and mean wave direction and how it varies for each sub-period can be seen in Table (4). In all cases there is a difference between the two but how well they correspond to each other can be seen in the percentage. The green highlighted rows show when the percentage for the differene-parameter is over 85 % to see which ones that has the best correspondence. The highest percentage has P2:6 with 94 % and therefore has waves that corresponds well to the wind direction. The lowest percentage has P3:4 with 26 % which shows a large difference between the mean direction of the wind and waves.

Table 4: The mean wind direction (WindD) and mean wave direction (WaveD) for the ADCP with the difference in percentage is displayed in the Table. A higher percentage of the parameter Difference means that the directions are closer to each other. The green highlight show which sub-periods that have a percentage above 85 %.

Period	Sub-period	Mean WindD [°]	Mean WaveD [°]	Difference
1	1	109	95	87 %
	2	188	168	89 %
2	1	215	176	81 %
	2	220	182	82 %
	3	205	182	83 %
	4	225	182	80 %
	5	210	184	87 %
	6	134	127	94 %
3	1	236	179	75 %
	2	198	165	83 %
	3	264	166	63 %
	4	204	54	26 %
	5	211	173	81 %
	6	214	146	68 %
4	1	169	157	92 %
	2	219	165	75 %
	3	246	179	73 %
	4	196	106	54 %
	5	177	118	67 %

5.3 Wave-induced turbulence

In Table 5 it is shown how the long- and short-distance waves were divided into two groups depending on degree of direction. This was conducted to make a comparison between the two types of waves.

Table 5: The division between the long-distance waves and the short-distance waves.

	Long-distance waves	Short-distance waves
Degree of direction	0° - 225°	225° - 0°

After dividing the data into the two categories, it was detected that all the waves, except for one time, were coming from the long-distance, 0°-225°. A hint for this result can also be seen in Fig. (7) & (8). Since this was the case, a comparison between the long- and short-distance waves and which one that lead to enhanced turbulence events was not conducted.

5.4 Parameterization

The calculated correlation coefficients between eps and $Terray$ and the difference between eps and $Terray$ for the upper 5 meters for each sub-period is shown in Table (6). The sub-periods highlighted in purple are the same sub-periods in Table (3) that are highlighted in purple, that show when the correlation coefficient are higher than 0.5 in both cases (R_{WS} & R_{Hs}). It can be seen that these sub-periods also present the lowest number of $Diff_{Terray}$. The curve for eps and $Terray$ and how the highlighted sub-periods vary with depth in relation to each other is displayed in Fig. (9). In this Figure it can also be seen that $Terray$ explains the measured turbulens best compared to LOW and $B0$. The difference between eps and LOW, called $Diff_{LOW}$ is also shown in Table (6) which in all cases is higher than $Diff_{Terray}$. This also shows that the $Terray$ parameterization is closer to the measured turbulence, as seen in the graphs (Fig. (9)). That this is the case, can be seen in the percentage which also is higher for $Diff_{LOW}$ compared to the percentage for $Diff_{Terray}$. This represents the difference in percentage between the measured turbulence and the calculated turbulence.

Table 6: The table shows the correlation coefficient between the measured turbulence, eps, and the calculated turbulence with the Terray parameterization, $Terray$, and the difference between eps and $Terray$ with the corresponding percentage.

| Period	Sub-period	R_{Terray}	$Diff_{Terray}$ $[m^2s^{-3}]$	$Diff_{Terray}$ $[\%]$	R_{LOW}	$Diff_{LOW}$ $[m^2s^{-3}]$	$Diff_{LOW}$ $[\%]$
1	1	0.99	$6.10 \cdot 10^{-5}$	98	0.96	$6.18 \cdot 10^{-5}$	99
	2	0.96	$-2.31 \cdot 10^{-5}$	38	0.95	$5.49 \cdot 10^{-5}$	91
2	1	0.95	$1.16 \cdot 10^{-4}$	88	0.91	$1.30 \cdot 10^{-4}$	99
	2	0.86	$6.53 \cdot 10^{-5}$	88	0.91	$7.37 \cdot 10^{-5}$	99
	3	0.87	$7.05 \cdot 10^{-5}$	74	0.78	$9.32 \cdot 10^{-5}$	98
	4	0.98	$1.14 \cdot 10^{-4}$	92	0.98	$1.24 \cdot 10^{-4}$	99
	5	0.99	$5.98 \cdot 10^{-5}$	90	0.99	$6.55 \cdot 10^{-5}$	99
	6	0.98	$2.35 \cdot 10^{-5}$	68	0.95	$3.36 \cdot 10^{-5}$	97
3	1	0.79	$5.87 \cdot 10^{-5}$	70	0.83	$8.16 \cdot 10^{-5}$	98
	2	0.76	$4.90 \cdot 10^{-5}$	91	0.85	$5.31 \cdot 10^{-5}$	99
	3	0.97	$1.97 \cdot 10^{-4}$	93	0.98	$2.11 \cdot 10^{-4}$	99
	4	0.86	$6.98 \cdot 10^{-5}$	99	0.95	$7.04 \cdot 10^{-5}$	99
	5	0.95	$3.20 \cdot 10^{-5}$	84	0.99	$3.73 \cdot 10^{-5}$	98
	6	0.91	$1.34 \cdot 10^{-5}$	66	0.98	$1.99 \cdot 10^{-5}$	97
4	1	0.85	$5.82 \cdot 10^{-5}$	93	0.90	$6.18 \cdot 10^{-5}$	99
	2	0.87	$9.54 \cdot 10^{-5}$	90	0.92	$1.05 \cdot 10^{-4}$	99
	3	0.69	$9.13 \cdot 10^{-5}$	86	0.81	$1.05 \cdot 10^{-4}$	99
	4	0.97	$4.63 \cdot 10^{-5}$	91	0.98	$5.05 \cdot 10^{-5}$	99
	5	0.86	$2.74 \cdot 10^{-5}$	43	0.99	$6.11 \cdot 10^{-5}$	95
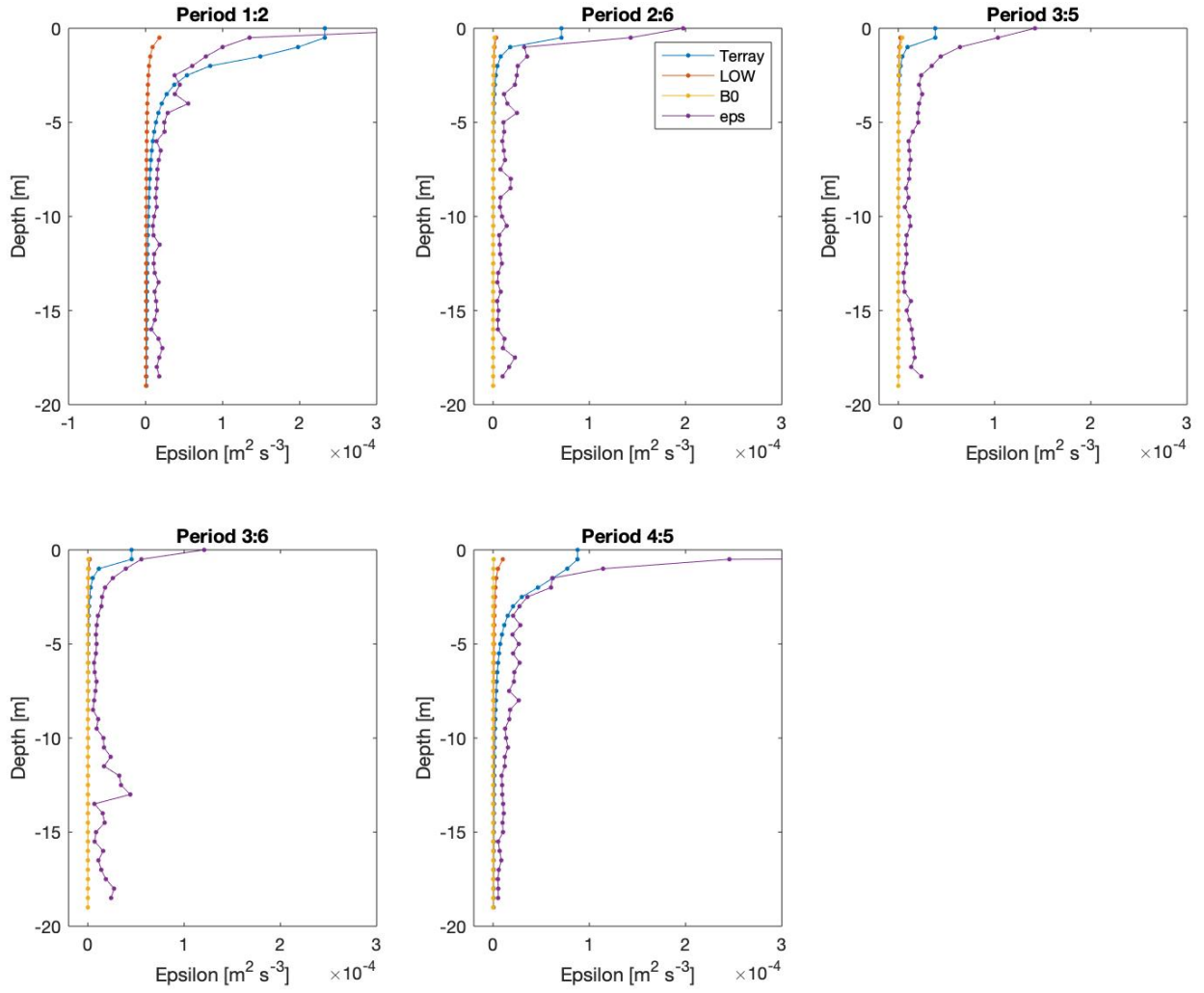
Figure 9: Depth variation of eps and the parameterizations for the selected sub-periods. The blue line show the $Terray$ parameterization, the orange line show the LOW parameterization, the yellow line show the $B0$ parameterization and the purple line show the measured turbulence eps.

The ratio between measured ϵ, called eps, and parameterized turbulence at each depth can be seen in Fig. (10). A value of 1 means perfect agreement whereas a value above 1 means under-prediction and a value below 1 means over-prediction. The $Terray$ parameterization under-predicts the measured turbulence in all cases since it is larger than 1. This also applies for the LOW parameterization. For the $B0$ parameterization the calculated turbulence is over-predicted at some depths, where it is smaller than 1, and also shows the biggest fluctuations. In most of the cases it can be seen that the fluctuations looks bigger with depth, which is caused because the turbulence is smaller here and therefore brings larger errors.
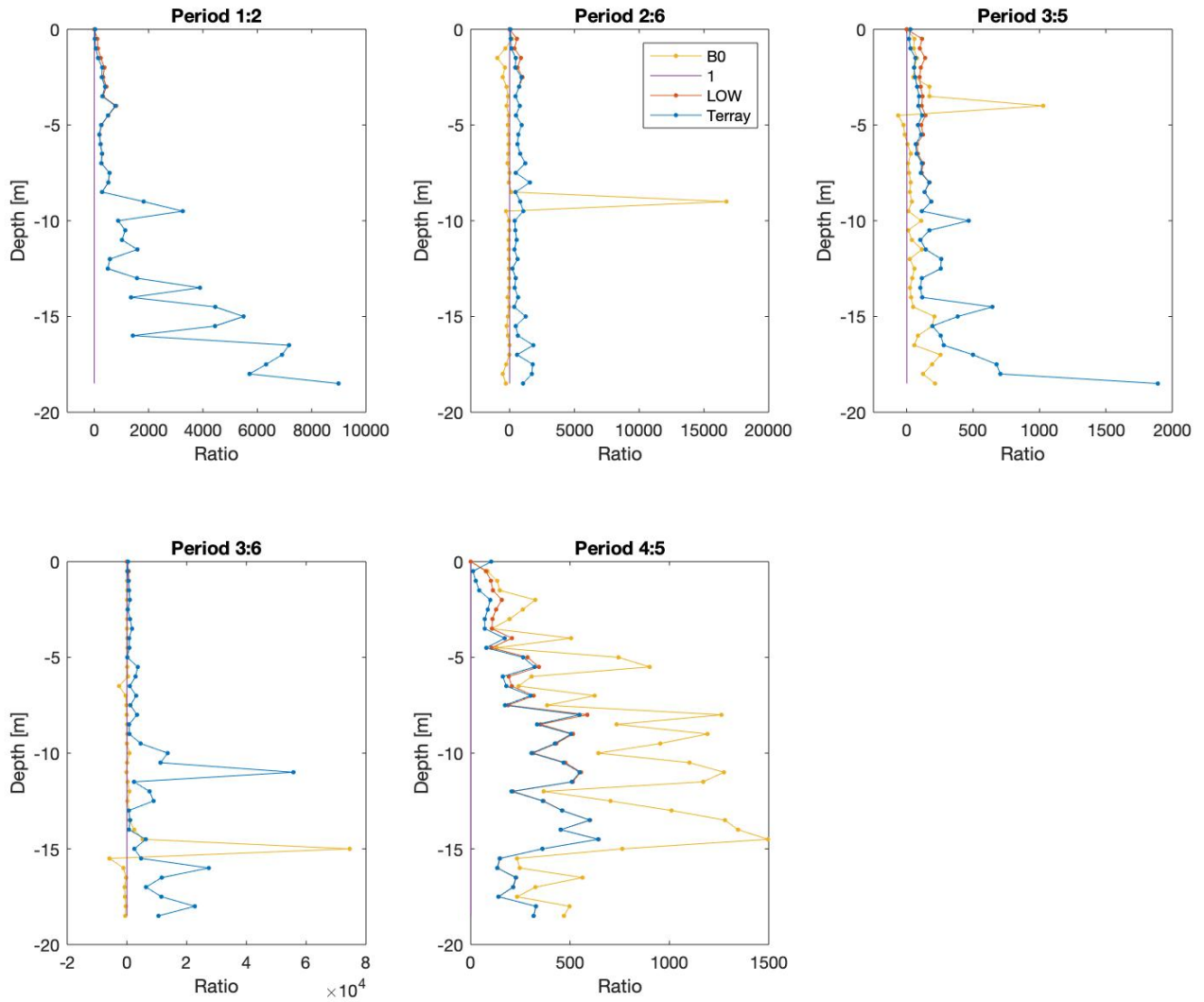
Figure 10: The ratio between measured turbulence (*eps*) and parameterized turbulence (*Terray*, *LOW* and *B*0) over the depth for each of the chosen sub-periods. The purple line at 1 illustrates a perfect agreement between measured and parameterized turbulence.

6 Discussion

6.1 Driving mechanisms for generation of enhanced turbulence events

To find the dominant driving mechanism for enhanced turbulence events at the surface wind, waves and buoyancy were investigated. Due to a lack of radiance data, buoyancy was excluded from the analysis. Instead, it was investigated if the wind, creating only shear drag explained by *LOW*, or wind and waves combined, explained by *Terray*, was the main driving mechanism for enhanced turbulence.

From Table (3) five sub-periods (P1:2, P2:6, P3:5, P3:6 & P4:5), highlighted in purple, were chosen for a more detailed analysis. They were chosen since both R_{WS} and R_{Hs} had a value higher than 0.5, which is a factor that suggests that the turbulence during these times is best described by wind and waves combined. The threshold at 0.5 was chosen since a delimitation had to be done among the sub-periods to facilitate the analysis. These sub-periods were therefore the sub-periods chosen for a more detailed investigation.

One sub-period (P1:1), highlighted in blue, had its R_{WS} equal to 0.5, which could be a evidence that this sub-period is best described by wind alone since it had a low correlation coefficient for R_{Hs} (0.19). It is also the sub-period with the lowest $\overline{WS}$ (4.96 m/s) which lies beneath the threshold discussed in Section 2.4.2 at 6 m/s. How the wind speed change over the sub-period can be seen in Fig. (5) and Appendix (A.2). From this, a peak that reaches over 6 m/s can be detected, but otherwise it is below this wind speed. As a cause of this it also has the lowest H_s (0.15 m). The waves are small and are probably not breaking either since the wind speed are below 6 m/s (Scalon & Ward, 2016) during most of the sub-period. The water surface could therefore be seen as a flat rigid 'wall' that is used in the *LOW* parameterization (Kantha & Clayson, 2000). What contradicts this theory is that R_{Terray} has a higher value than R_{LOW} and that $Diff_{Terray}$ has a lower value than $Diff_{LOW}$ in Table (6). The difference between these two parameters is however smaller than in most of the sub-periods. The Diff-parameter describes how large the difference between the parameterized turbulence and the observed turbulence is. The correlation coefficient describes how well the parameters follow each other, but if the Diff-value is larger than expected this could mean that parameterization does not accurately explain the reality, and some other parameters are missing to get a good parameterization of the observed turbulence.

Four sub-periods (P2:1, P2:5, P3:4 & P4:1), highlighted in yellow in Table (3), had a higher value than 0.5 for R_{Hs}, but lower than 0.5 for R_{WS}. This occurs four times compared to one for R_{WS}. From the correlation coefficient alone, it could be seen that the wind and waves combined lead to more occasions (five times) related to the $xld4m$, which describes the turbulence at the surface. Thereafter, the waves that have four occasions with a correlation coefficient higher than 0.5 compared to the wind with only one occasion with a correlation coefficient at 0.5. But only studying this parameter can be misleading, because if Fig. (5) and Appendix (A.2) are analyzed it can be seen that $xld4m$ has a delay compared to WS and H_s in some of the sub-periods. That meaning that the peak in $xld4m$ does not occur at the same time as the peak in WS or H_s. This results in a lower correlation coefficient and could therefore be misleading and leading to take the conclusion that the wind and waves do not lead to increased $xld4m$.

P1:2 and P4:5 (Fig. 6) both indicate that turbulence in the water can be delayed to peaks in wind and waves, that is that the increase in $xld4m$ is not occuring at the same time as an increase in wind speed and waves. In these two sub-periods there are a large peak in WS with a corresponding peak in H_s. The increase in $xld4m$ that can be seen in both cases is delayed and appear after the wind speed has decreased again after its peak. In P1:2 there is one peak in $xld4m$ that has its maximum when the wind has decreased from its maximum around 18 m/s to around 6 m/s. For P4:5 increased turbulence is observed at the same time as the wind speed and H_s, but has maximal levels of turbulence when the wind speeds are lower and the size of H_s has decreased. But what contradicts

27

this theory is that in sub-period P2:6, P3:5 and P3:6 $xld4m$ follows the WS well with peaks at the same time. The difference in these sub-periods compared to P1:2 and P4:5 is however that they have a lower value for the $\overline{H_s}$, the mean value of H_s, under the sub-period, and not as distinct peaks for the H_s that can be seen changing over time in Fig. (5). This could explain that the same pattern of a delayed increase in turbulence does not appear in these sub-periods (P2:6, P3:5, P3:6). That this is the case can be seen in Table (3) where, of the five purple highlighted sub-periods, P1:2 and P4:5 has a higher value of $\overline{H_s}$. Sub-period P1:2 and P4:5 does also have the highest $\overline{WS}$ among the purple highlighted sub-periods that also would cause larger H_s. What also can be mentioned is that in some of the sub-periods the standard deviation are relatively large (Table 3). For the wind speed, this can be seen in for example sub-period P1:2, P2:6, and P4:5 for the chosen sub-periods. This could suggest that there are some cases in the time period with very strong wind speeds that differs from the mean wind speed, which then could lead to increased turbulence. This may be why it is the selected sub-periods that show higher standard deviations. The pattern with higher standard deviations for the chosen sub-periods can be seen to some extent for H_s as well.

When comparing the result for Diff_{Terray} and Diff_{LOW} it could be seen that the $Terray$ parameterization showed a better comparison to the measured eps in all sub-periods. It is interesting to compare this result with the results $Esters\ et\ al.$ (2018) described in their article. They stated that the LOW parameterization described the ocean surface turbulence more accurately than the $Terray$ parameterization in open ocean conditions.

The difference (Diff) and the correlation coefficient was calculated only for the upper 5 m. This was because it could be seen that there was a significant increase in turbulence deeper in the water column for some sub-periods (Fig. 4). This turbulence was not connected to the surface turbulence and could therefore affect the result for the analysis of the surface turbulence. This thesis focuses on how the interactions with the atmosphere drive the surface turbulence, which makes deeper turbulence, not linked to the surface, out of the scope for this thesis. How the turbulence changed with depth, for eps, $Terray$, LOW and $B0$ can be seen in Fig. (9) and Appendix (A.3). The chosen sub-periods represent the overall pattern of how the three parameterizations relate to the observed turbulence over the water column. It can be detected that $Terray$ described eps most accurately in all cases, followed by LOW and thereafter $B0$. The result showed thus different results than what was shown by $Esters\ et\ al.$ (2018), that LOW described turbulence more accurately than $Terray$.

It can also be seen that the parameterized turbulence was under-predicted in all cases except for sub-period P1:2. This could indicate that some factors are missing in the parameterizations. This could also show that different parameterizations are appropriate to use during different conditions, so this has to be adapted to the situation to get a result that reflects the real turbulence events. For example, that the $Terray$ parameterization gives better results in high wind speeds with waves that correspond to the changes in wind speed.

6.2 Direction of Wind and Waves

Formation of waves depends on wind speed, fetch length, and the amount of time the wind blows consistently over the fetch (Ainsworth, 2018), where the fetch and amount of time with consistent winds will be affected by the islands. Refraction of waves can also play a role in how the wave direction distribution is around the islands and appear at the location for the ADCP and the Wave rider. The comparison between the wind direction and wave direction showed that there were some differences between the two. Both the ADCP and the Wave rider showed signs of being sheltered by the islands, Gotland and Östergarnsholm, since they had directions from which no large waves were measured. The ADCP measured waves up to a lower degree of direction since the instrument measured closer to Gotland (Fig. 2) compared to the Wave rider. That the ADCP is more affected by the islands can also be seen by the magnitude of H_s. The ADCP measured smaller H_s to a higher extent than the Wave rider, which is a possible cause of being sheltered by the islands.

Another reason for the differences between the ADCP and the Wave rider could be that they measure the wave direction in different ways. The Waver rider gives the direction of the maximum in the measured wave spectrum while the ADCP gives the mean degree of the direction of the whole wave spectrum.

As stated before, there are differences in the wind directions and wave directions. The differences can be seen both in the wind and wave roses (Fig. (7)), but also in the scatterplots (Fig. (8)). The reason for this can be explained by the impact the islands have on the formation of waves and how they travel. Wind does not get as affected since it blows above the ground and does not get interrupted to the same extent as waves.

The wind direction and wave direction did not correspond perfectly since there were directions that had not detected any waves even if the wind was in that direction, which also can be seen in the R^2-value shown in Fig. (8), a) ADCP: 0.18 & b) Wave rider: 0.05. When the ADCP measures the wave height and direction and what the main direction is, there is going to be a spectrum of waves where several wave directions are included. The most frequent wave direction is then the direction that will be determined for that specific point in time. So it can be that the waves coming from the short-distance sector of direction are outnumbered by the waves coming from the long-distance and that is why the waves from short-distance are not presented. Most of the largest H_s came however from the open ocean when both the wind and waves came from around 100°, from southeast (Fig. 8 & Fig. 2).

It is also interesting that the correlation coefficient between the wind direction and wave direction for the Wave rider is substantially lower than for the ADCP. By considering the discussion on the difference between the wave and wind direction from the ADCP earlier the islands is seen as the main cause for the difference. But following this hypothesis, the Wave rider would show better correlation to the wind direction since it is located further away from the islands than the ADCP and therefore get a longer fetch length and get less affected by the islands. The cause for the lower value of R^2 for the Wave rider could be a consequence of the outliers that can be seen in Fig. 8b).

From Table (4) it can also be seen that the mean wave direction in all sub-periods is coming from the long-distance, compared to the two cases that the mean wind direction is coming from the short-distance (P3:1 & P3:3).

6.3 Wave-induced turbulence

The research question "*What kind of waves creates the enhanced turbulence events to a greater extent? Long- or short-distance waves?*" can not be answered in the way that was planned. Since the waves only came from the direction mentioned as the long-distance, it can be said that the waves that contributed to near-surface turbulence were long-distance waves. The reason for waves only coming from the direction 0° - 225° is probably because the islands, Östergarnsholm and Gotland, shelters the location where the ADCP is situated, as discussed in the previous section. This can also be proven by comparing the wave roses (Fig. 7). The distribution of directions measured by the ADCP and the Wave rider looks similar, but the Wave rider has waves coming from a higher degree of direction than the ADCP and has a greater amount of larger H_s. This is due to the positions with the islands, the Wave rider has a location further away from the islands and is therefore not as sheltered as the location for the ADCP.

Waves are an important factor for the upper-ocean mixing, both breaking and non-breaking waves, as stated by e.g. *Wu et al. (2015)*. In this thesis, it can not be answered if the long- or short-distance waves are the the most important for the enhanced turbulence or knowing if the waves break or not. What can be said is that for this location the turbulence will most likely be affected in a greater extent by long-distance waves.

7 Conclusions

The aim of this thesis was to gain knowledge about surface ocean turbulence in the Baltic Sea and its formation. This was conducted by an analysis of turbulence data collected in the Baltic Sea and meteorological parameters during the same time period. For the thesis, four research questions were posed and investigated.

It was investigated how the surface turbulence, illustrated by $xld4m$ that shows the depth to which active turbulence reaches, changed over time compared to wind and waves during the sub-periods. By combining this with how the parameterizations described turbulence, it was found that wind and waves together described surface turbulence most accurate. This conclusion was based on the fact that there were more cases where waves or wind and waves combined had better correlation coefficent with $xld4m$ than just with wind (Table 3). Thus, one can argue that waves are a more important source of energy to create surface turbulence than wind alone.

In addition, when studying the parameterization it could be seen that the $Terray$ parameterization was closer to the observed turbulence compared to the LOW parameterization. This was seen both by studying the Diff-values (Table 6) and the graphs showing the turbulence over the water column (Fig. 9). A conclusion from this is that the $Terray$ parameterization is closer to the measured turbulence and therefore describes the reality more accurate.

It was also found that the parameterizations, *Terray* and *LOW*, under-predicted the measured turbulence in most cases. The only occasion when this was not the case was during a condition with high wind speeds with correlated waves.

As a result of the sheltering from Östergarnsholm and Gotland a difference between the wind and wave direction was found. This could affect the result and therefore differ from how the turbulence would look in the open ocean.

Because of the location of the ADCP, there were no measured short-distance waves in the data during the investigated time period. The mean direction was below 200° in all cases except for one occasion, which made it impossible to investigate if long- or short-distance waves contributes most to surface turbulence.

7.1   Future work

For future research, it would be interesting to make similar research far away from the coast to see if the *Terray* parameterization describes the turbulence most accurately here as well. It could otherwise be that the *LOW* parameterization predicts the surface turbulence better in these open ocean conditions like it was stated by *Esters, et al.* (2018). But if this is not the case, maybe the *Terray* parameterization describes the surface turbulence better in the Baltic Sea.

It would also be interesting to see how $xld4m$ varies as a function of buoyancy. Since waterside convection mostly occurs during the night, a diurnal or seasonal dependence might be detected. The parameterization for $B0$ would perhaps look different illustrated in Fig. (9) as well.

By investigating each wave spectrum separately and choosing the long- and short-distance waves and comparing these to the enhanced surface turbulence, it would be interesting to see which type corresponds best to $xld4m$. This was out of the scope for this thesis because it would have been too time-consuming. But it could be interesting to investigate this to see what type of waves creates enhanced turbulence events to a greater extent and if there is a difference.

References

Ainsworth, T. (2018). When Do Ocean Waves Become 'Significant'? A Closer Look at Wave Forecasts. *Mariners Weather Log.* 50(1).

Alderton, D. & Elias, S. A. (2021). Coastal Mapping and Monitoring. In: Trembanis, A., Lundine, M. & McPherran K. (eds). *Encyclopedia of Geology.* Volume 2. 251-266. Oxford: Academic Press. https://doi.org/10.1016/B978-0-12-409548-9.12466-2

Belcher, S. E., Grant, A. L.M., Hanley, K. E., Fox-Kemper, B., Van Roekel, L., Sullivan, P. P., Large, W. G., Brown, A., Hines, A., Calvert, D., Rutgersson, A., Pettersson, H., Bidlot, J.-R., Janssen, P. A.E.M., Polton, J. A. (2012). A global perspective on Langmuir turbulence in the ocean surface boundary layer. *Geophysical Research Letters.* 39 (L18605). ISSN 0094-8276 doi: 10:1029/2012GL052932

Burchard, H. & Umlauf, L. (2018). *Marine Turbulence.* Leibniz Institute for Baltic Sea Research Warnemünde.

Brainerd, K. & Gregg, M.C. (1993). Diurnal Restratification and Turbulence in the Oceanic Surface Mixed Layer 1. Observations. *Journal of Geophysical Research.* 98(C12), 22645-22656.

Brainerd, K.,E & Gregg, M.C. (1995). Surface mixed and mixing layer depths. *Deep Sea Research Part I: Oceanographic Research Papers.* 42(9), 1521-1543. https://doi.org/10.1016/0967-0637(95)00068-H

Cushman-Roisin, B. (2019). *Environmental Fluid Mechanics.* New York: John Wiley Sons, Inc.

Esters, L., Breivik, Ø., Landwehr, S., ten Doeschate, A., Sutherland, G., Christensen, K. H., Bidlot, J.-R., Ward, B. (2018). Turbulence Scaling Comparisons in the Ocean Surface Boundary Layer. *JGR Oceans.* 123 (3), 2172-2191. https://doi.org/10.1002/2017JC013525

Fossum, H. E., Wingstedt, E. M. M., Reif, B. A. P. (2013). A model for the viscous dissipation rate in stably stratified, sheared turbulence. *Geophysical Research Letters.* 40 (14), 3744-3749. https://doi.org/10.1002/grl.50663

Gargett, E. & Grosch, E. (2014). Turbulence Process Domination under the Combined Forcings of Wind Stress, the Langmuir Vortex Force, and Surface Cooling. *Journal of Physical Oceanography.* 44(1), 44–67. https://doi.org/10.1175/JPO-D-13-021.1

Gemmrich, J. R. & Farmer, D. M. (2004). Near-Surface Turbulence in the Presence of Breaking Waves. *Journal of Physical Oceanography.* 34 (5), 1067–1086. https://doi.org/10.1175/1520-0485(2004)034¡1067:NTITPO¿2.0.CO;2

Glegg, S. & Devenport, W. (2017). *Aeroacoustics of Low Mach Number Flows.* Pages 185-200. Academic Press.

Google Maps, (n.d). *Google Maps, Gotland.* `https://www.google.se/maps/place/623+66+Gotland/@57.4479814,18.3338431,9z/data=!4m5!3m4!1s0x46f7136945a81403:0x33ab84c3bc7e586f!8m2!3d57.370624!4d18.699161` [20-03-2021]

Hendriks, M.R. (2010). *Introduction to Physical Hydrology.* New York: Oxford University Press.

ICOS (n.d.). *Östergarnsholm.* `https://www.icos-sweden.se/Ostergarnsholm` [26-02-2021]

Kantha, L. H. & Clayson, C. A. (2000). *Small Scale Processes in Geophysical Fluid Flows*, volume 67. Academic Press. DOI: 10.1016/S0074-6142(00)80077-7

Lombardo, C.P. & Gregg, M.C. (1989). Similarity Scaling of Viscous and Thermal Dissipation in a Convecting Surface Boundary Layer. *Journal of Geophysical Research.* 94(C4), 6273-6284.

Lorke, A., & F. Peeters (2006). Toward a Unified Scaling Relation for Interfacial Fluxes. *Journal of Physical Oceanography.* 36 (5), 955–961. doi:10.1175/JPO2903.1.

McGillicuddy, D.J. & Franks, J.S.P. (2019). Models of Plankton Patchiness. *Encyclopedia of Ocean Sciences.* 5, 536-546. https://doi.org/10.1016/B978-0-12-409548-9.11610-0

National Centers for Environmental Prediction/National Weather Service/NOAA/U.S. Department of Commerce. 1994, updated monthly. NCEP/NCAR Global Reanalysis Products, 1948-continuing. Research Data Archive at NOAA/PSL: `/data/gridded/data.ncep.reanalysis.html` [01-02-2020]

National Geographic (2019). *Ocean.* `https://www.nationalgeographic.org/encyclopedia/ocean/` [2021-04-19]

Richardson, L.F. (1922). *Weather prediction by numerical process.* Cambridge University Press.

Rutgersson, A., Pettersson, H., Nilsson, E., Bergström, H., Wallin, M. B., Nilsson, E. D., Sahlée, E., Wu, L. Mårtensson, E. M. (2020). Using land-based stations for air–sea interaction studies. *Tellus A: Dynamic Meteorology and Oceanography*, 72(1), 1-23. DOI: 10.1080/16000870.2019.1697601

Ryden, B. (2009). *Radiative Gas Dynamics.* Ohio: The Ohio state University.

Scanlon, B. and Ward, B. (2016). The influence of environmental parameters

on active and maturing oceanic whitecaps. *JGR: Oceans.* 121(5), 3325-3336. oi.org/10.1002/2015JC011230.

Terray, E. A., Donelan, M. A., Agrawal, Y. C., Drennan, W. M., Kahma, K. K., Williams III, A. J., Hwang, P. A. and Kitaigorodskii, S. A. (1996). Estimates of Kinetic Energy Dissipation under Breaking Waves. *Journal of Physical Oceanography.* 26(5), 792–807.

Thorpe, S.A. (2004). Recent developments in the study of oceanic turbulence. *Annual Reviews.* 32(119), 91-109. https://doi-org.ezproxy.its.uu.se/10.1146/annurev.earth.32.071603.152635

Thorpe, S. A. (2007), *An Introduction to Ocean Turbulence*, New York: Cambridge University Press.

Tokoro, T., Kayanne, H., Watanabe, A., Nadaoka, K., Tamura, H., Nozaki, K., Kato, K. and Negishi, A. (2008). High gas-transfer velocity in coastal regions with high energy-dissipation rates. *Journal of Geophysical Research.* 113(C11).

Trembanis, A., Lundine, M. & McPherran K. (2021). Coastal Mapping and Monitoring. *Encyclopedia of Geology.* 2 Pages 251-266

Wu, L., Rutgersson, A., and Sahlée, E. (2015). Upper-ocean mixing due to surface gravity waves. *Journal of Geophysical Research.* 120(12), 8210-8228, doi:10.1002/ 2015JC011329.

A Appendix

A.1 Buoyancy fluxes
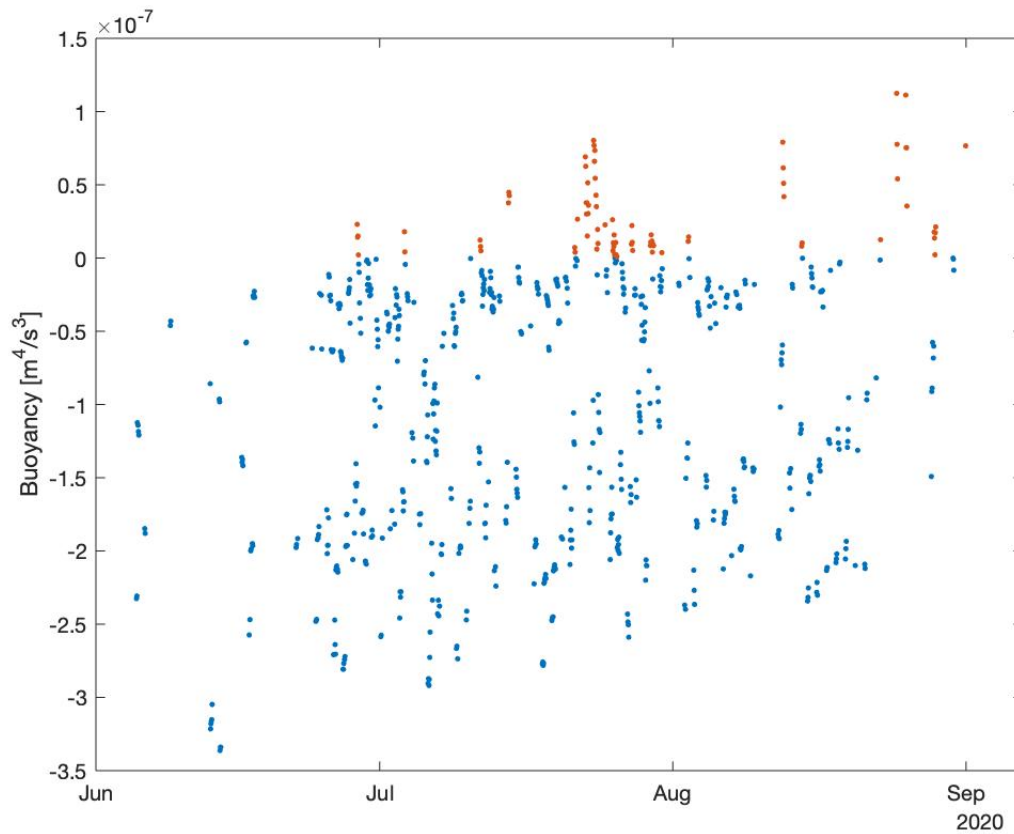
Figure 11: The buoyancy flux over the chosen time period. The orange points illustrates positive values.

A.2 Changes in WS, H_s and $xld4m$ over the sub-periods
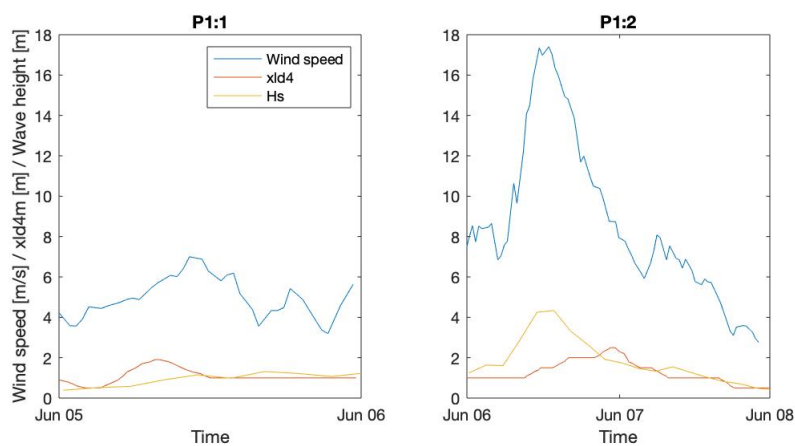
Figure 12: Sub-periods for period 1 divided into separate graphs. H_s is multiplied with a factor of 2.

35
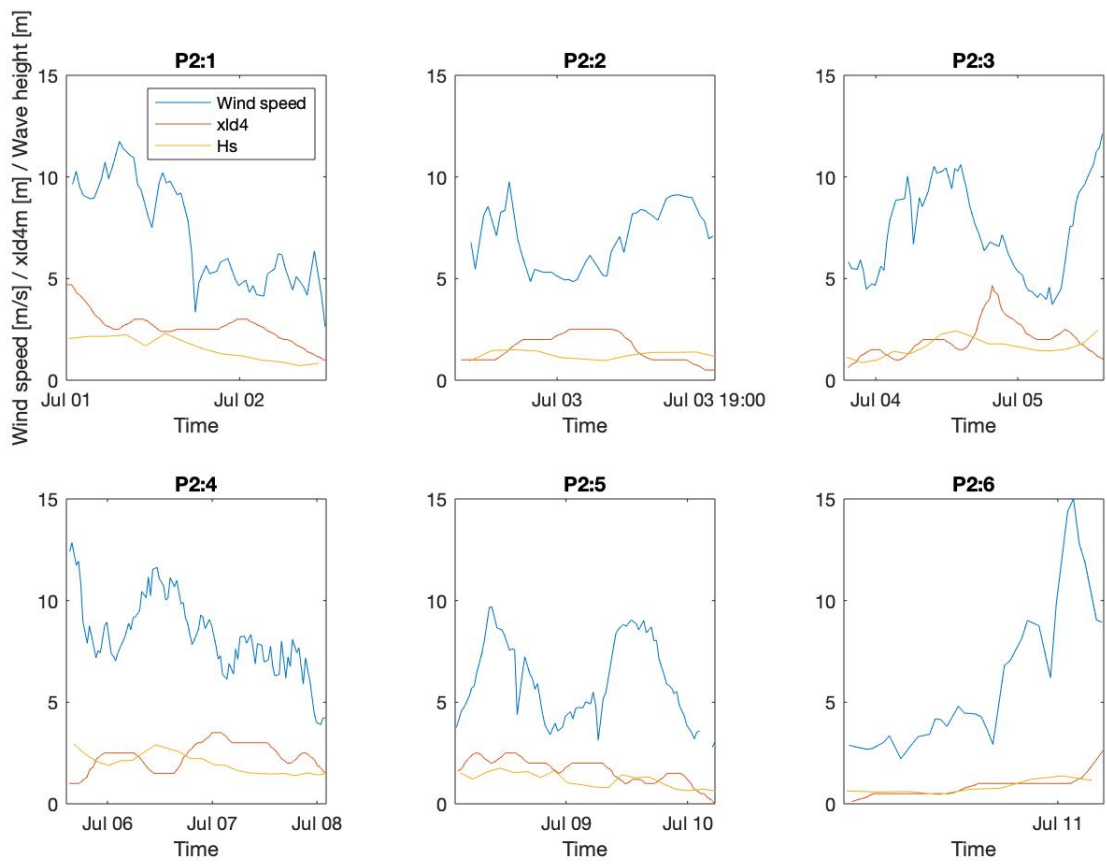
Figure 13: Sub-periods for period 2 divided into separate graphs. H_s is multiplied with a factor of 2.
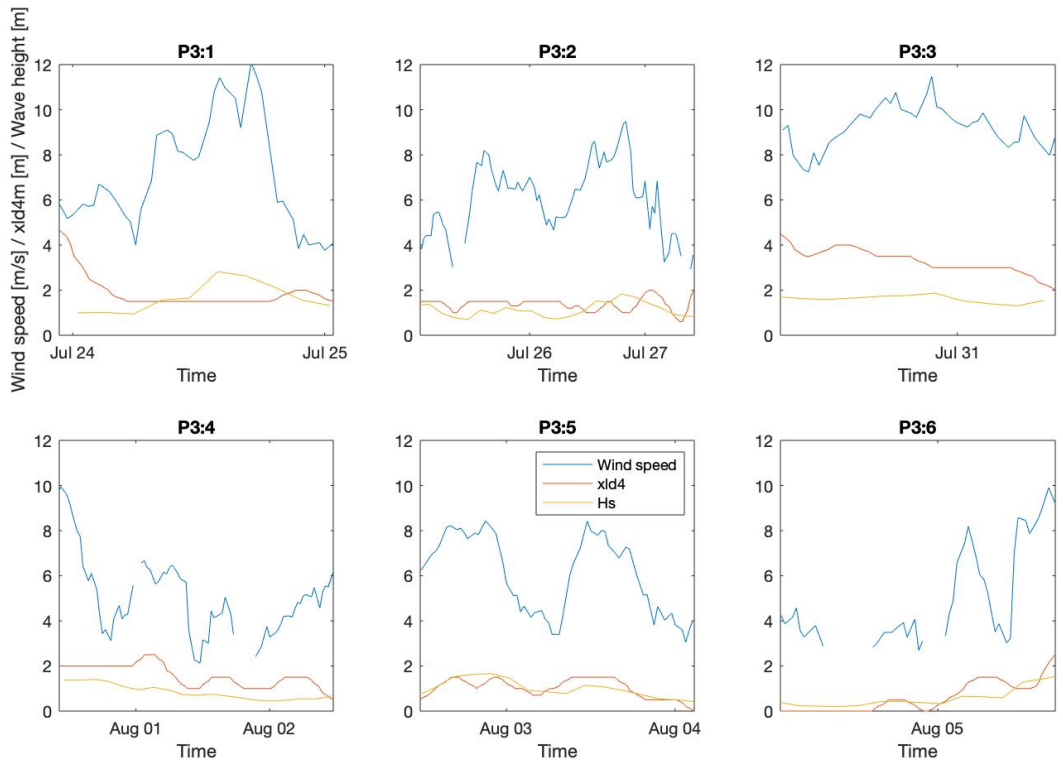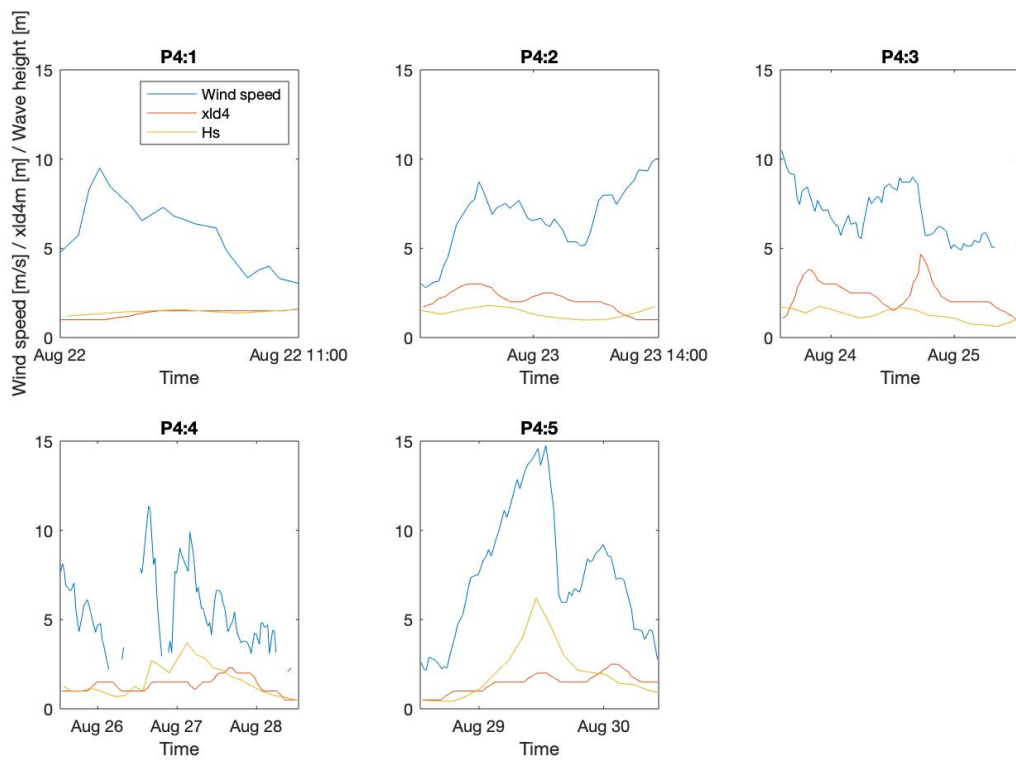

Figure 14: Sub-periods for period 3 divided into separate graphs. H_s is multiplied with a factor of 2.

Figure 15: Sub-periods for period 4 divided into separate graphs. H_s is multiplied with a factor of 2.

A.3 Turbulence over the water column for the different sub-periods
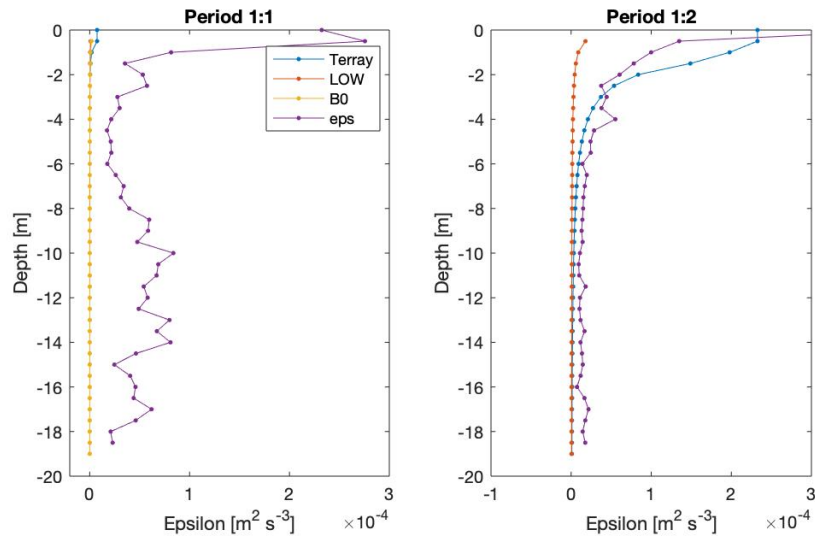
Figure 16: Measured turbulence (eps) and the parameterized turbulence ($Terray$, LOW and $B0$) averaged for each sub-period over depth.
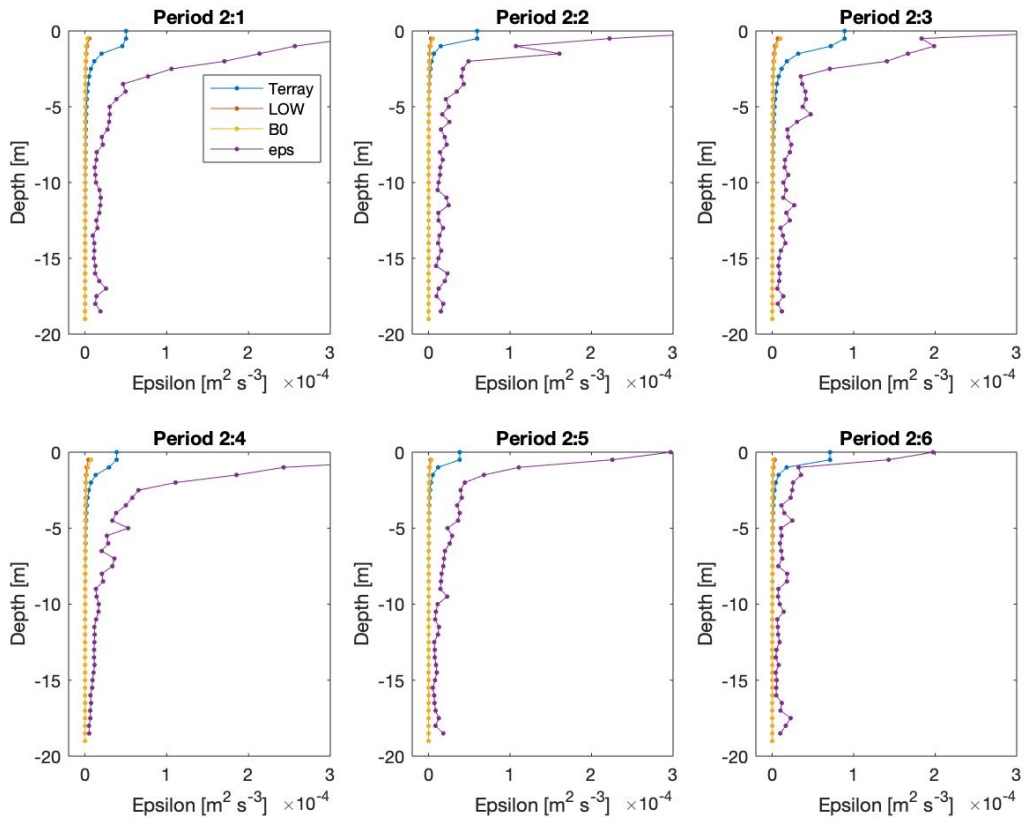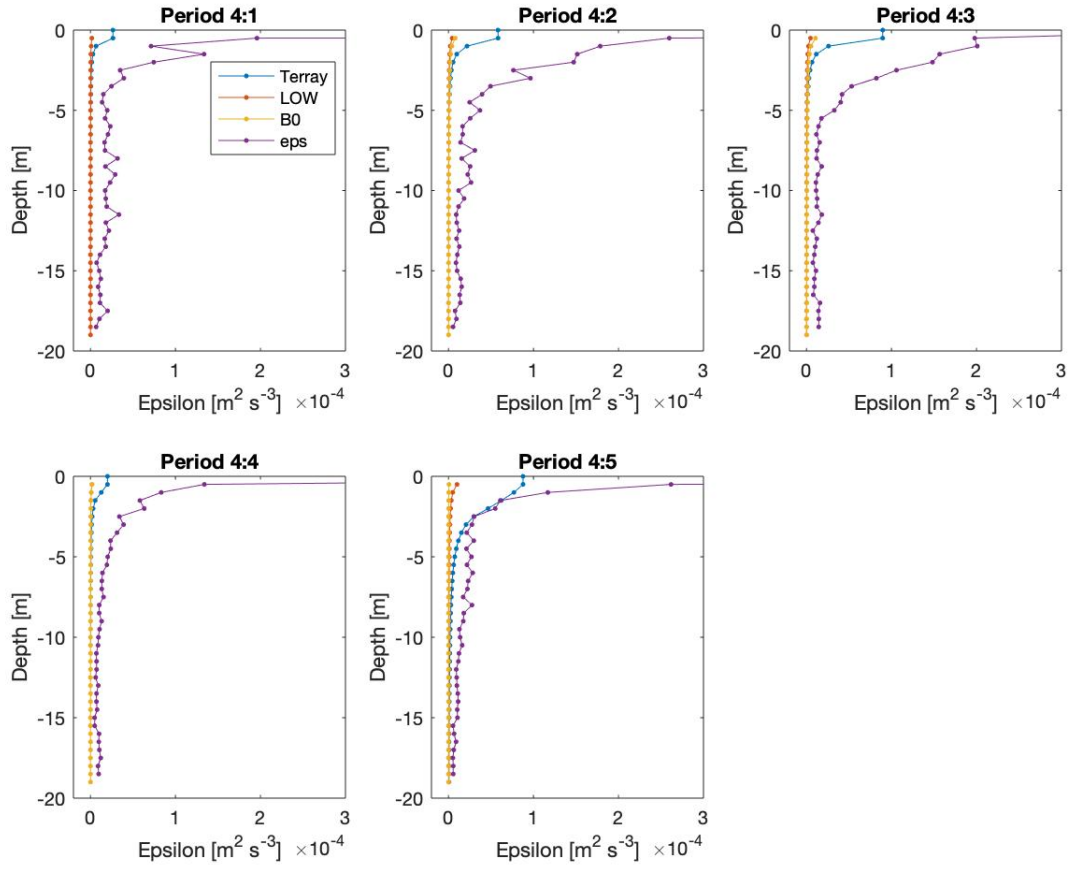
Figure 17: Measured turbulence (*eps*) and the parameterized turbulence (*Terray*, *LOW* and *B*0) averaged for each sub-period over depth.
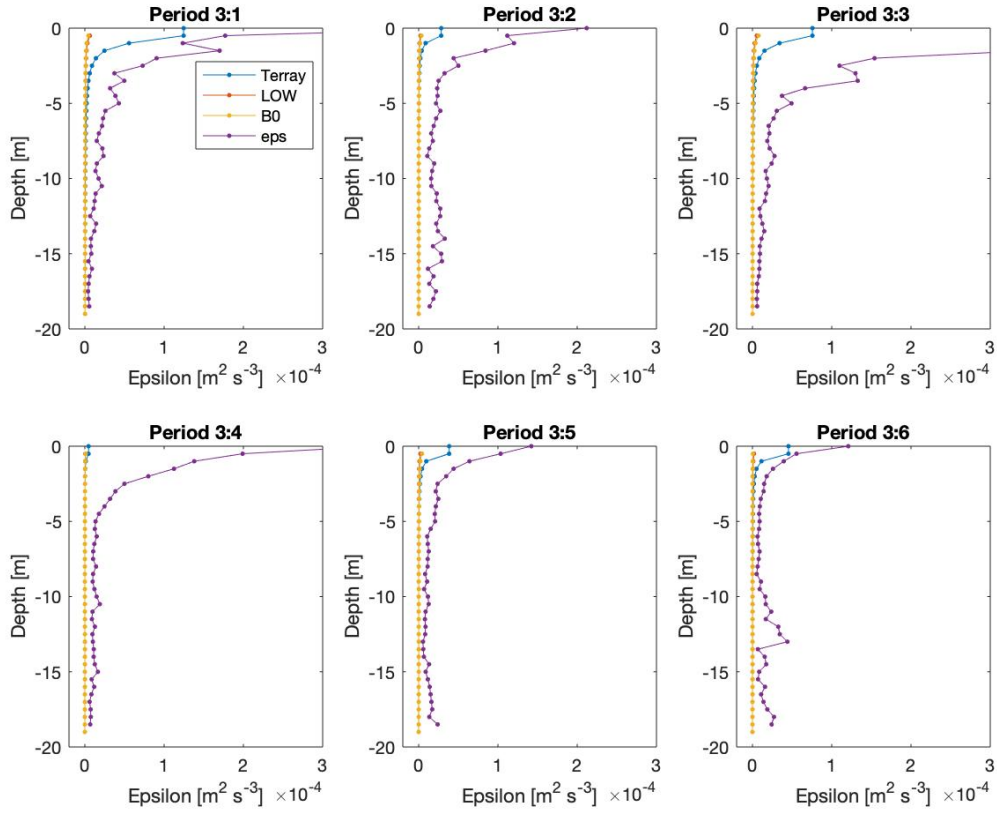
Figure 18: Measured turbulence (*eps*) and the parameterized turbulence (*Terray*, *LOW* and *B*0) averaged for each sub-period over depth.

Figure 19: Measured turbulence (*eps*) and the parameterized turbulence (*Terray*, *LOW* and *B*0) averaged for each sub-period over depth.

A.4 The ratio between the measured turbulence and the parameterized turbulence over the water column
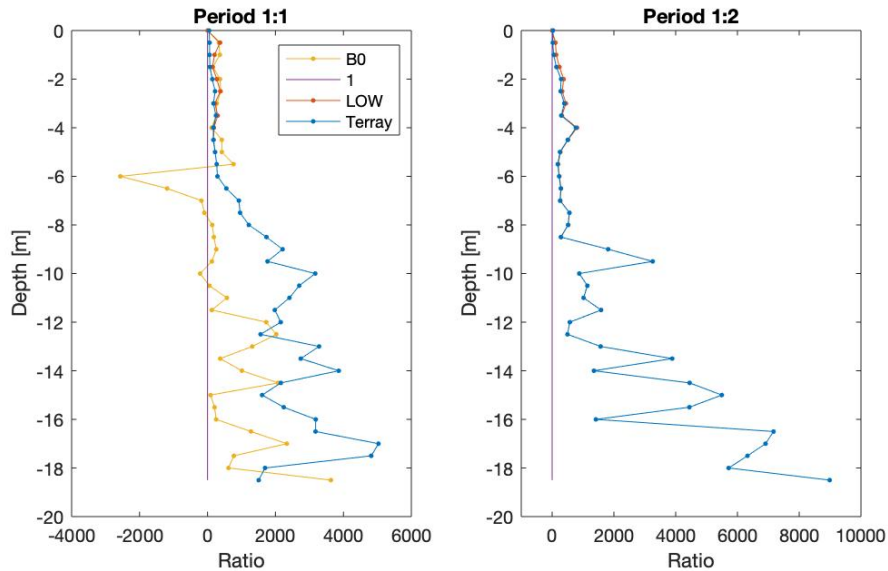
Figure 20: The ratio between measured turbulence (*eps*) and parameterized turbulence (*Terray*, *LOW* and *B*0) over the depth for each sub-period.
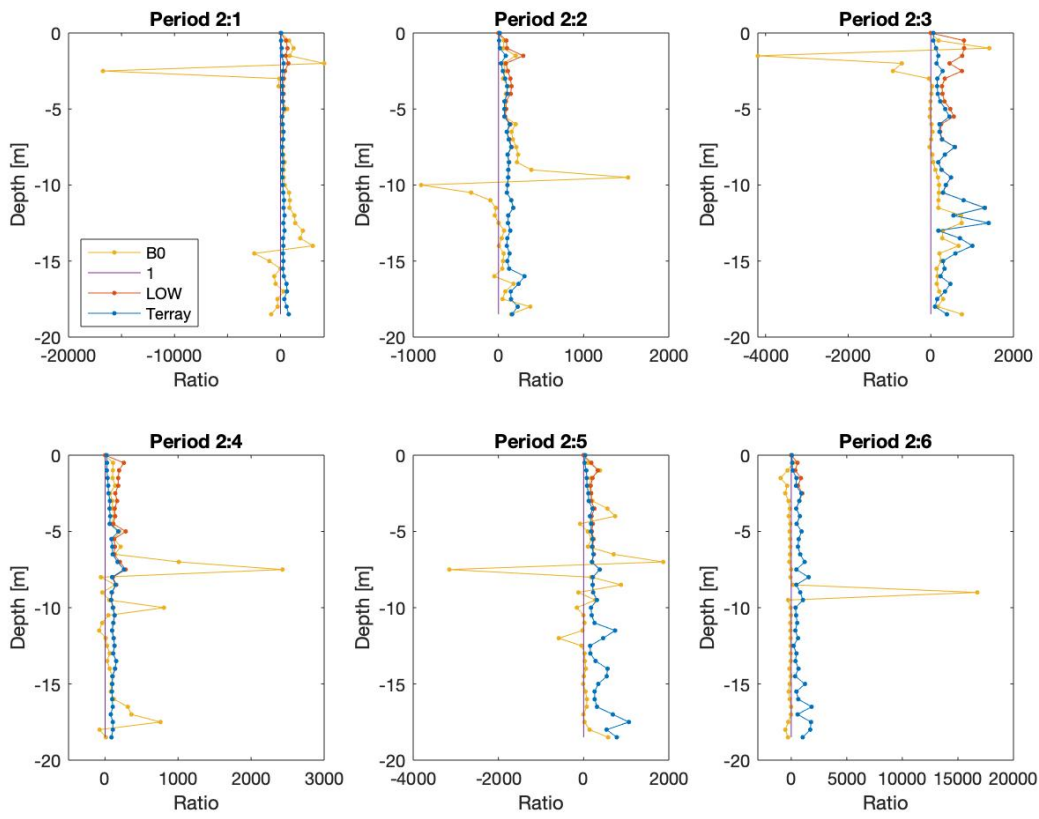
Figure 21: The ratio between measured turbulence (eps) and parameterized turbulence ($Terray$, LOW and $B0$) over the depth for each sub-period.
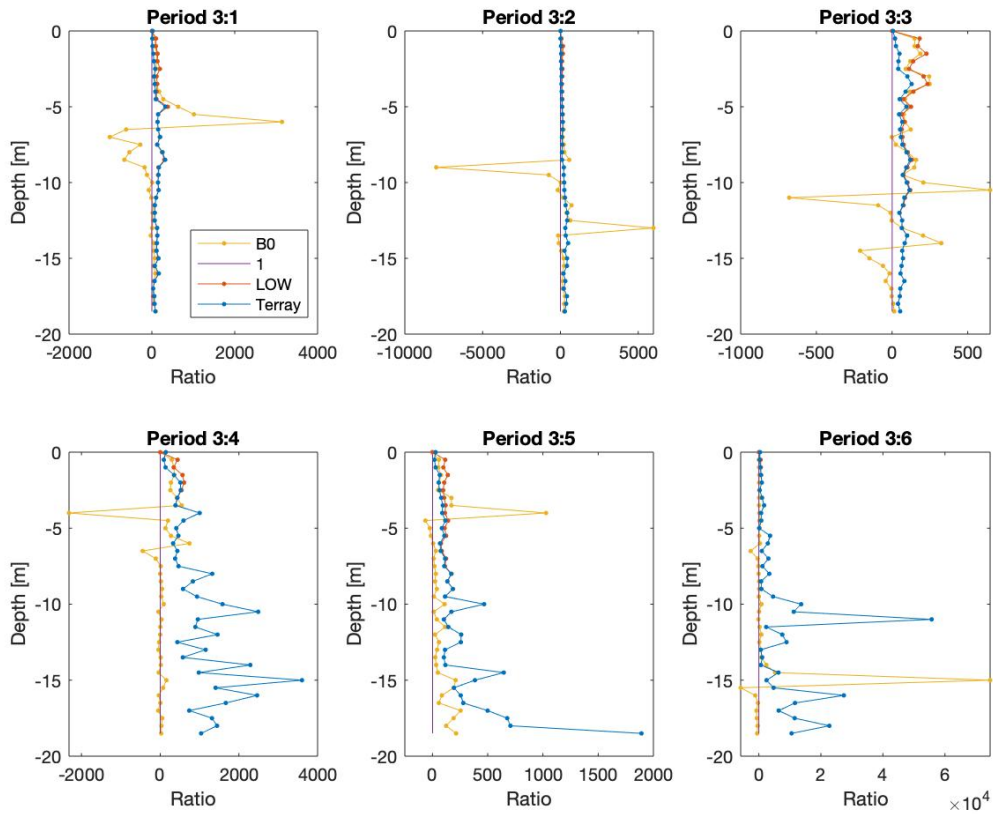

Figure 22: The ratio between measured turbulence (eps) and parameterized turbulence ($Terray$, LOW and $B0$) over the depth for each sub-period.
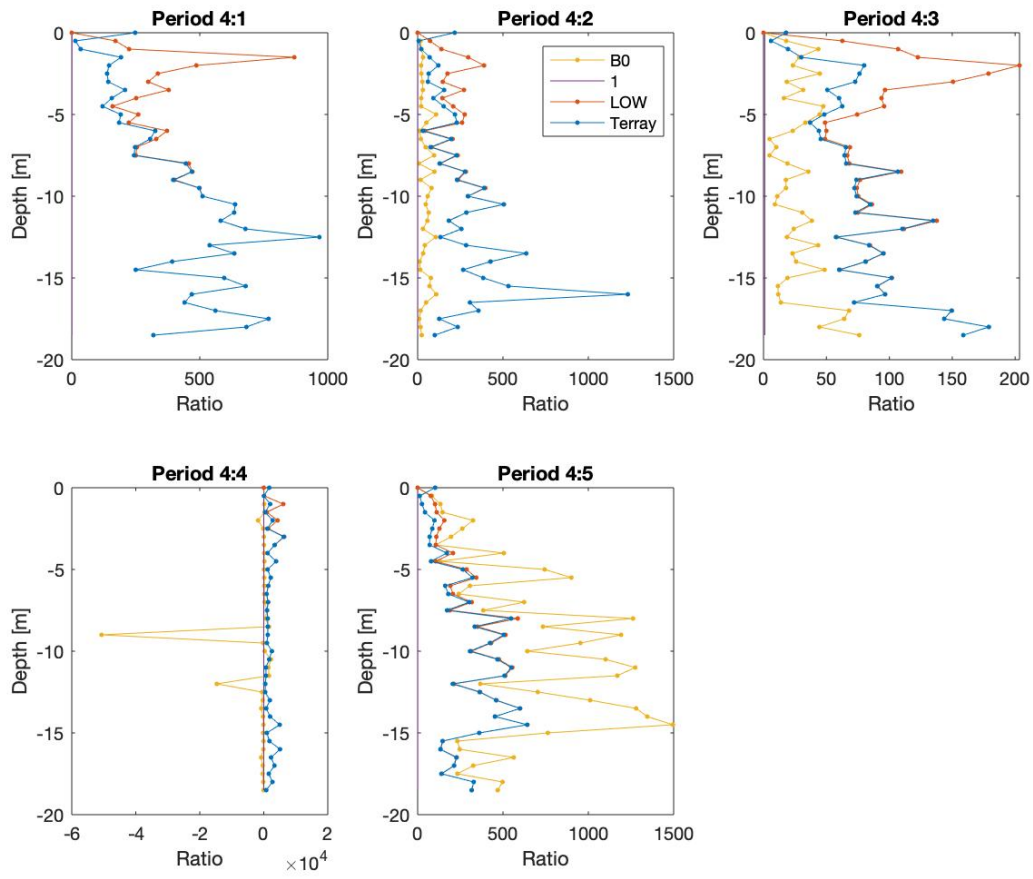
Figure 23: The ratio between measured turbulence (eps) and parameterized turbulence ($Terray$, LOW and $B0$) over the depth for each sub-period.